https://doi.org/10.5194/cp-2022-60
Preprint. Discussion started: 16 August 2022

Climate of the Past Discussions

Late Neogene nannofossil assemblages as tracers of ocean circulation and paleoproductivity over the NW Australian shelf

Boris-Theofanis Karatsolis[1] and Jorijntje Henderiks[1]

[1]Department of Earth Sciences, Uppsala University, Uppsala, 752 36, Sweden

Correspondence to: Boris Theofanis Karatsolis (boris.karatsolis@geo.uu.se)

Abstract.

Late Miocene to Pliocene sediments from the NW Australian shelf provide unique records of paleoclimatic variations under warmer-than-present conditions. During the period from 6-3.5 million years ago (Ma), the area was dominated by warm, tropical waters supplied by an intensified, uninterrupted Indonesian Throughflow and characterised by prevailing humid conditions and increased precipitation. Despite the available information regarding the general paleoclimatic conditions, little is known about the concurrent regional ocean circulation patterns and the relative intensity of seasonally flowing boundary currents, such as the Leeuwin Current. Recent investigations of sediments recovered from the shelf during International Ocean Discovery Program (IODP) Expedition 356, have produced a number of well-dated time-series that cover the late Neogene and can therefore assist with more detailed reconstructions. In this study, we investigate two astronomically-tuned calcareous nannofossil records from IODP Sites U1463 and U1464 that can help us trace and understand long-term changes in ocean circulation and seasonality, as well as their effect on nutrient replenishment in the upper photic zone. By looking into shifts in the dominant species within the nannofossil assemblage, and comparing them with paleotemperature gradients between the NW Australian shelf and the eastern Indian Ocean, we identify the main periods of change in stratification and nutrient availability that occurred over the continental shelf. Our results indicate a significant change in ecological and oceanographic regime that occurred across the Miocene to Pliocene boundary (5.4–5.2 Ma), which can be attributed to an increase in seasonality and an overall intensification of the upper water column mixing over the shelf. Major changes in the nannofossil assemblages that reflect broader-scale processes and evolutionary events, such as the extinction of *Sphenolithus* spp. (~3.54 Ma) and the termination of the late Miocene to early Pliocene biogenic bloom in the eastern Indian Ocean (4.6-4.4 Ma), occurred long after this regional regime shift.

https://doi.org/10.5194/cp-2022-60
Preprint. Discussion started: 16 August 2022

Climate of the Past Discussions

1 Introduction

Marine phytoplankton are sensitive indicators of current and past climatic change, with coccolithophores being the most extensively studied, because of their long, abundant, and mostly well-preserved record in shallow marine and deep-sea sediments since the late Triassic. Through their fossilised calcareous platelets (coccoliths and nannoliths), these organisms record both regional paleoclimatic and paleoceanographic changes, but also global processes such as evolution and basin-wide changes in ocean chemistry (Beaufort et al., 1997; Bolton et al., 2016; O'Dea et al., 2014; Thierstein and Young, 2004). Because of this interplay of regional and global signals preserved in the sediment record, nannofossil assemblage studies come with a set of challenges, especially in highly dynamic environments across continental shelves. In such areas, coccolithophore communities may be significantly different than open ocean marine settings, owing to the influence from parameters such as seasonal water column stratification and tidal mixing (Sharples et al., 2009; Van Oostende et al., 2012), as well as variations in river runoff and nutrient input (Harlay et al., 2010; Poulton et al., 2014). This further complicates the task of using the nannofossil assemblage to consistently differentiate between signals of regional paleoclimatic forcing and broad-scale evolutionary trends and changes in the ocean's nutrient availability.

The NW Australian shelf serves as an important test-case to try and tackle these challenges, because of its position within the dynamic climate system of the Indo-Pacific warm pool and near the only remaining equatorial warm water valve. Modern ocean circulation in the area is controlled by a variation in intensity of the Indonesian Throughflow (ITF) and the Leeuwin Current (LC). The ITF is the warm surface current that transports water from the Western Pacific Warm Pool (WPWP) into the Indian Ocean (Du and Qu, 2010; Gordon et al., 1997; Figure 1). The LC is a boundary current that is sourced by the ITF and transports warm water southwards (Figure 1), with significant implications for fisheries and the persistence of tropical biota in the high latitudes of western and southwestern Australia (e.g. Kendrick et al., 2009 and references therein). Its strength varies seasonally, with the strongest flow being observed during austral winter, when latitudinal steric height gradients are steeper (e.g. Godfrey and Ridgway, 1985; Ridgway and Godfrey, 2015). Interannually, stronger (weaker) LC is linked to La Niña (El Niño) conditions, with a mean annual transported volume of 4.2 Sv (3 Sv) (e.g., Feng et al., 2003, 2009). Additionally, this flow is known to consist of warm-core anticyclonic eddies that can promote phytoplankton production across the western Australian shelf (Koslow et al., 2008; Thompson et al., 2007). The NW Australian shelf is a source area of the LC, contributing to its total volume through a surface current called the Holloway Current (HC; D'Adamo et al., 2009; Holloway and Nye, 1985), that flows south-westward along the shelf. Weak upwelling events have been observed in the area both during summer and winter months, when westerly winds are strong enough to overcome the steric height gradient (Holloway and Nye, 1985). Modern observational data and forecasts (E.U. Copernicus Marine Service Information) show that during austral winter, when LC is strong, the NW Australian shelf area is characterised by a mixed layer deepening, which reaches ~100m and occurs

https://doi.org/10.5194/cp-2022-60
Preprint. Discussion started: 16 August 2022

Climate of the Past Discussions
Open Access
EGU

because of an invigoration of the upper water column mixing. At the same time, chlorophyll-a increases in the surface layer, driven by an increase in water column cooling and advective mixing (Figures 2, 3).

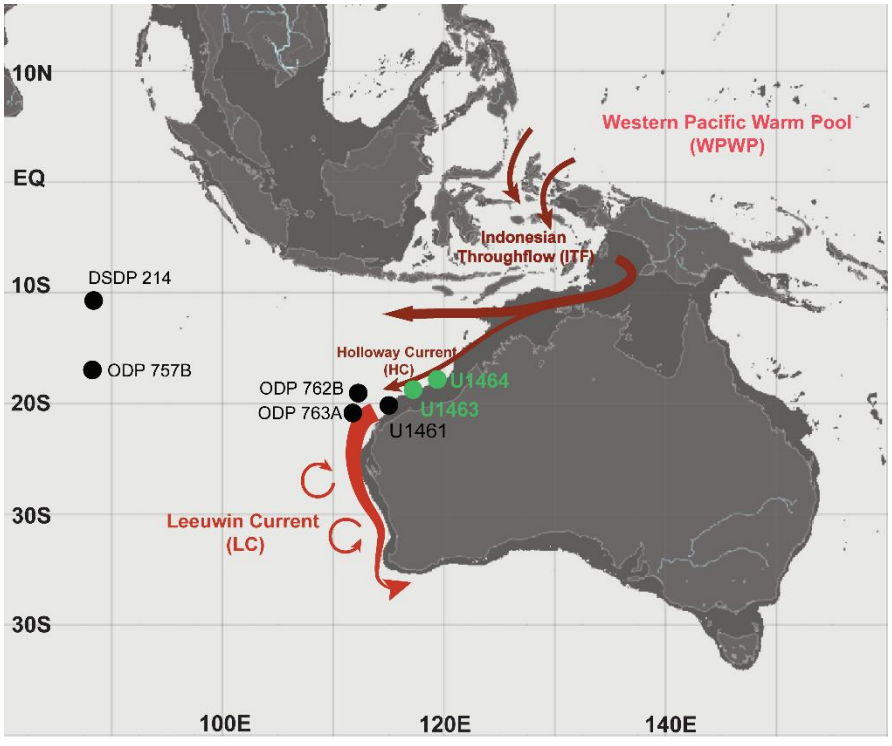

Figure 1: Modern bathymetric map indicating shelfal environments (<200m depth; dark grey) and site locations. IODP Sites U1463 and U1464 (NW Australian shelf; this study) are shown with green circles. IODP Site U1461 (NW Australian shelf), ODP 763A and ODP 762B (Eastern Indian Ocean), as well as ODP 757B and DSDP 214 (equatorial Indian Ocean), are discussed in the text and shown in black circles. Also shown, the main surface oceanography of the Indo-Pacific region (dark red lines) and main path of the LC (lighter red line; adapted by (Auer et al., 2019; Gallagher et al., 2009) and the HC, which in this study are considered as one. Base map was generated using the ocean data visualization tools of E.U. Copernicus Marine Service Information (MYOCEAN PRO).

Information on the existence and strength of the LC in the latest Miocene and Pliocene remains limited, although a possibly active LC has been inferred from upper water column temperature and primary productivity reconstructions at its source area (IODP Expedition 356 Site U1461; Figure 1) for the interval spanning from 6-4 Ma (He et al., 2021). During that time, increased river runoff and humid conditions were prevailing in the area, under an intensified Indonesian Throughflow (ITF) (Auer et al., 2019; Christensen et al., 2017; He et al., 2021; Karatsolis et al., 2020). Previous investigations have demonstrated that the nannofossil assemblage has the potential to reflect ocean circulation changes in the area and closely track the ITF source water variations and LC activity during the late Pliocene to Pleistocene (Auer et al., 2019). At the same time, evidence for broader changes in the ocean nutrient budget comes from the opportunistic, fast-growing (bloom-forming) species of the assemblage, which significantly decreased their fluxes from 4.6–4.4 Ma, recording the end of the late Miocene to early Pliocene biogenic bloom in warm over the NW Australian shelf (Karatsolis et al., 2020, 2022).

https://doi.org/10.5194/cp-2022-60
Preprint. Discussion started: 16 August 2022

Climate of the Past Discussions
Open Access
EGU

In this study, we aim to further constrain the latest Miocene to early Pliocene ITF and LC history, by identifying the key changes in the calcareous nannofossil assemblage. To achieve that, we extend the nannofossil record from IODP Site U1463 (Auer et al., 2019) back to ~5.7 Ma and present one more astronomically-tuned record from IODP Site U1464, that is located ~100 km but in a different basin, dating back to ~6 Ma (Gallagher et al., 2017: Karatsolis et al, 2020). We evaluate the use of a ratio between three abundant taxonomic groups (genera) as an index to trace long-term shifts in water-column stratification and regional ocean circulation. Comparison with newly constrained temperature gradients between the NW Australian shelf and the eastern Indian Ocean further assists in identifying the possible underlying mechanisms for the observed changes. Finally, nannofossil evidence is put in a broader perspective in an effort to differentiate between signals that reflect basin-wide or global changes in nannoplankton evolution and the ocean's nutrient budget, and those that occurred due to regional ocean circulation and intensity of seasonal variations. Such decoupling of regional signals from overlying global patterns is crucial when using the nannofossil assemblage to reconstruct the evolution of the LC, as well as other boundary currents and ocean circulation patterns in dynamic shelfal environments.

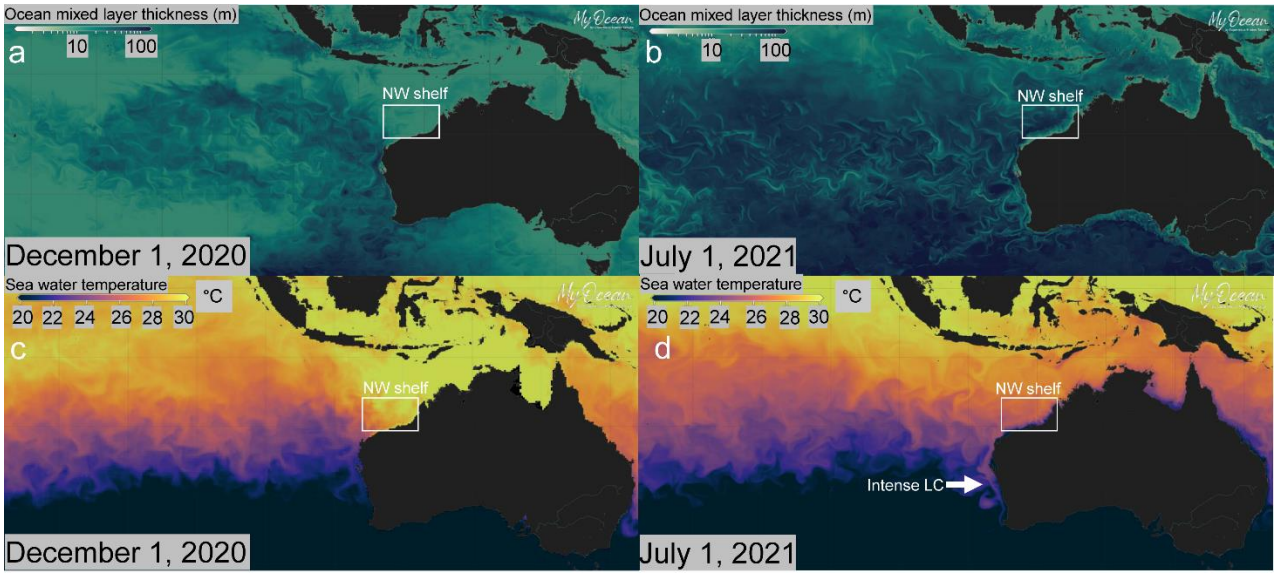

Figure 2: Present-day ocean circulation maps of the southeastern Indian Ocean area for the 1st of December 2020 (austral summer; a-c) and 1st of July 2021 (austral winter; b-d). LC is weak during austral summer causing reduced depth of the mixed layer and increased stratification (a) and SST (c) in the NW Australian shelf. LC intensifies during austral winter, while water column mixing in the eastern Indian Ocean increases and SST decreases in the NW Australian shelf area (b,d); at the same time, it transports warmer surface waters further to the south (d). The sea surface cooling effect observed in shelfal environments during July is less pronounced further offshore. Maps were generated using the ocean data visualization tools of E.U. Copernicus Marine Service Information (MYOCEAN PRO) and dataset layer GLOBAL_ANALYSIS_FORECAST_PHY_001_024 (https://doi.org/10.48670/moi-00016) and GLOBAL_ANALYSIS_FORECAST_BIO_001_028 (https://doi.org/10.48670/moi-00015).

https://doi.org/10.5194/cp-2022-60
Preprint. Discussion started: 16 August 2022

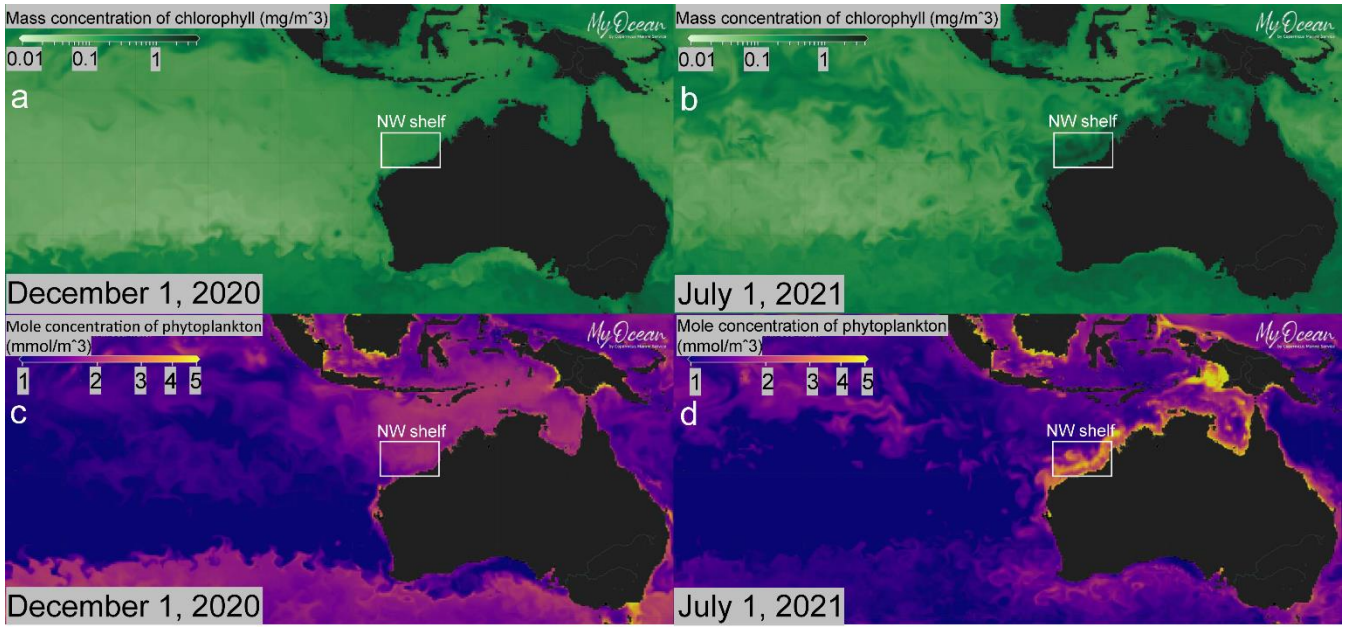

Figure 3: Present-day ocean productivity maps of the southeastern Indian Ocean area for the 1st of December of 2020 (austral summer; a-c) and 1st of July of 2021 (austral winter; b-d). Reduced LC and water column stratification during austral summer leads to low concentrations of chlorophyll (a) and phytoplankton (c) in the NW Australian shelf area. Intense LC and storm track activity during austral winter leads to increased water column mixing in the NW Australian shelf and significantly higher chlorophyll (b) and phytoplankton concentrations (d). Maps were generated using the ocean data visualization tools of E.U. Copernicus Marine Service Information (MYOCEAN PRO) and dataset layer GLOBAL_ANALYSIS_FORECAST_BIO_001_028 (https://doi.org/10.48670/moi-00015).

2 Material and Methods

2.1 Nannofossil Counts

IODP Expedition 356 Sites U1463 (145 m water depth; 18°59′S, 117°37′E) and U1464 (270 m water depth; 18°03.9115′S, 118°37.8935′E) (Figure 1) yielded a stratigraphic succession from the late Miocene to the early Pleistocene, with abundant, moderately preserved calcareous nannofossils. Note that the late Miocene to Pliocene sediments were deposited at much greater depths than the current water depth suggests, mirroring at the time of deposition middle/outer shelf to upper bathyal conditions (Christensen et al., 2017; Gallagher et al., 2017). A total of 209 samples (104 samples from IODP Site U1463 and 105 from U1464) were prepared for micropaleontological analysis, with a sampling interval of ~1.5m (at least one sample per core section). Sample preparation followed the ‘drop technique’ (Bordiga et al., 2015). For each sample, 5 mg of dried bulk sediment was weighed and initially diluted with 20 mL of ammonia-buffered water. After short sonification, the suspension was passed through a 63 µm-meshed sieve and further diluted to three different final concentrations (bulk-weight equivalent concentrations of ~0,125 mg/mL; 0,08 mg/mL; 0,04 mg/mL). Subsequently, 1.5 mL of well-mixed suspension was placed on a cover slip with a high-precision micropipette, and the sample was dried on a hotplate at 60°C. Finally, cover slips were

https://doi.org/10.5194/cp-2022-60
Preprint. Discussion started: 16 August 2022


Climate of the Past Discussions

mounted on glass slides with Norland Optical Adhesive (NOA61) and cured under a UV light source for approximately half an hour.

Micropaleontological analysis was conducted using polarized light microscopy at 1000 × magnification, with at least 300 specimens counted and identified at genus level per sample. Coccoliths within the *Reticulofenestra* and *Gephyrocapsa* genera were further classified by size categories of <3µm (small), 3-5µm (medium) and >5µm (large). Samples from different initial concentrations were selected, based on the abundance of nannofossils in the samples. Confidence intervals for nannofossil relative abundance were calculated using the binomial error function (95% CIs) in PAST 4 freeware (Hammer et al., 2001), as suggested by Suchéras-Marx and others (2019). Subsequently, absolute abundances (in N/g) of the different genera and morphospecies were calculated using the following equation (e.g., Koch and Young, 2007):

$$(1)\ \text{Abs. Abundance (AA)} = \frac{\mathrm{N}\times\mathrm{A}}{\mathrm{f}\times\mathrm{n}\times\mathrm{W}},$$

where A is the area of the cover slip (mm^2), N is the total number of nannofossils counted, f is the area of one field of view (FOV; mm^2), n is the number of FOV, and W is the equivalent dry bulk sediment weight on the cover slip (g). Reproducibility for the absolute abundance calculation is estimated to be ±10-15% (Bordiga et al., 2015).

Nannofossil fluxes were calculated following the formula:

$$(2)\ \mathrm{NAR} = \mathrm{AA} \times \mathrm{LSR} \times \mathrm{DBD},$$

where NAR stands for nannofossil accumulation rates (N/cm^2 kyr), AA is the absolute abundance of coccoliths (in N/g), LSR is the linear sedimentation rate (in cm/kyr) calculated between astronomically-tuned tie points and DBD is the dry bulk density of the sample (in g/cm^3). Nannofossil flux records older than 5.8 Ma at IODP Site U1464 were not considered, since they are potentially linked to the high sedimentation rates that were observed following the abrupt, late Miocene deepening of the Roebuck basin (Karatsolis et al., 2020). Despite that, relative abundances can still be considered to reflect changes in the assemblage and are therefore presented, extending the record at IODP Site U1464 back to ~6 Ma. All nannofossil data were placed on the tuned age models for U1463 and U1464, as presented by Groeneveld and others (2021) and Karatsolis and others (2020).

2.2 Correspondence analysis (CA) and Shannon Diversity Index (H)

Correspondence analysis (CA) and calculation of the Shannon Diversity Index (H) (Shannon, 1948) were conducted using PAST 4 freeware (Hammer et al., 2001). We applied CA to the nannofossil time series data, in order to compare samples of different age based on the relative abundance of species present in each sample (column principal with ages representing distinct columns). This allowed for identification and visualization of possible breaking points where species composition and the structure of the assemblage significantly changed through time. However, this ordination method does not provide measures of statistical significance, and therefore only serves to confirm, by observations in multivariate space, the main trends observed in the raw data. CA was chosen over Canonical Correspondence Analysis (CCA), because our time series do not include any additional environmental parameters (no environmental gradient extraction). The H index was calculated to spot

https://doi.org/10.5194/cp-2022-60
Preprint. Discussion started: 16 August 2022


Climate of the Past Discussions

shifts in nannofossil diversity and identify intervals of species overturn. The H index varies from 0 for assemblages consisting of a single species to high(er) values for assemblages with many species, but each represented by few individuals.

2.3 Stratification Index

A ratio between the three most common genera of the assemblage, namely bloom-forming *Reticulofenestra* and *Gephyrocapsa* species and *Sphenolithus* spp., was calculated to investigate relative changes in water column conditions. Species comprising this ratio are abundant throughout the record until the extinction of *Sphenolithus* spp. at ~3.54 Ma, while no long-term decreasing trend in the relative abundance of *Sphenolithus* was observed in the time preceding its last occurrence (Figure A1). The calculation followed the equation:

$$(3)\ \mathrm{NSI} = \frac{\mathrm{Sph}}{\mathrm{Sph}+(\mathrm{Rm}+\mathrm{Rs}+\mathrm{Gs})},$$

where Sph, Rm, Rs and Gs represent the relative abundances of *Sphenolithus* spp. medium-sized *Reticulofenestra* and small-sized *Reticulofenestra* and *Gephyrocapsa* species, respectively.

Of the nannofossil groups comprising this ratio, small sized *Reticulofenestra* species have been demonstrated to thrive in unstable conditions during the Pliocene, since they were favoured by more pronounced seasonality and tidal mixing (Auer et al., 2019; Ballegeer et al., 2012). With a similar ecological affinity, medium-sized *Reticulofenestra* species reflected neritic conditions with increased nutrient availability through local upwelling activity (Auer et al., 2019 and references therein). Small *Gephyrocapsa*, although also considered bloom-forming, highly opportunistic species, were adapted to warmer and more stratified water masses, as commonly inferred in subtropical continental margins (Auer et al., 2019; Boeckel and Baumann, 2008; Okada and Wells, 1997; Takahashi and Okada, 2000). *Sphenolithus* spp. on the other hand, although of complex paleocological affinity that ranges from low-latitude, oligotrophic warm waters (e.g., Gibbs et al., 2004; Haq, 1980; Haq and Lohmann, 1976) to restricted mesotrophic ocean masses (Wade and Bown, 2006), has been commonly grouped with *Discoaster* as characteristic of warmer, more stratified water conditions compared to the bloom-forming *Reticulofenestra* and *Gephyrocapsa* species (e.g. Gibbs et al., 2005; Haq and Lohmann, 1976). Similar ratios between "cool", mesotrophic species and "warmer", oligotrophic species have been used in the past for other geological periods. For example, the ratio between species of the genus *Toweius* with *Sphenolithus* and *Discoaster* has been used as a paleoenvironmental index for the Paleocene-Eocene thermal maximum (Gibbs et al., 2010). Species of the genus *Toweius* have been characterised as meso/eutrophic, having occupied a similar niche to the modern bloom-forming species (e.g. Bralower, 2002; Gibbs et al., 2010). Similarly, a ratio between *Reticulofenestra* species and *Florisphaera* has been used to monitor changes in the nutricline and thermocline during the Pleistocene (Flores et al., 2000). We therefore propose that the ratio of *Sphenolithus* spp. to bloom-forming species can serve as a useful indication of changes in water column mixing and nutrient availability and has the potential to record

https://doi.org/10.5194/cp-2022-60
Preprint. Discussion started: 16 August 2022

185 relative stratification above the NW Australian shelf during the latest Miocene to Pliocene. For this reason, we will be referring to this ratio as the nannofossil stratification index (NSI).

2.4 Paleotemperature proxies and gradient calculation

Paleotemperature gradients between three sites located in the eastern Indian Ocean (DSDP Site 214, ODP Site 763A) and the
190 NW Australian shelf (IODP Site U1461) (Figure 1), were calculated based on available estimates. At IODP Site U1461, proxy records include GDGT-based TEX_{86} temperature and alkenone-based $U^{k'}_{37}$ SST (He et al., 2021), spanning the interval from ~6-3.5 Ma. At ODP Site 763A and DSDP Site 214, available records consist of Mg/Ca derived SSTs from *Trilobatus sacculifer* foraminifera (Karas et al., 2009, 2011). Site-to-site temperature differences were calculated between samples with the closest assigned age. The median difference between closest ages for any pair of sites ranged between 0.1-3 kyr (Table D1), although
195 in one case, due to a gap of >200kyr in sample spacing at DSDP Site 214, this difference became 100kyr (~3.75-3.96 Ma) for gradients involving this site. However, this gap in paleotemperature estimate occurred towards the end of our studied interval and therefore does not limit our potential to investigate possible links to sustained changes in the nannofossil assemblage that occurred across the Miocene/Pliocene boundary and between 4.6–4.4 Ma. All the above-mentioned proxies have been used to infer paleotemperature in the sea surface (upper 50 m) or integrated upper water column (upper 200 m), although some
200 discrepancies and possible biases do exist that will be addressed in the discussion.

3 Results

3.1 Nannofossil relative abundances and fluxes

205 Calcareous nannofossils are very abundant and moderately preserved throughout the studied interval. Coccolith NAR and relative abundances reveal highly similar patterns at both sites, with bloom-forming *Reticulofenestra* (<5μm) and *Gephyrocapsa* (<3μm) species always dominating the assemblage (combined ~60-97%; Figure A1). The smallest bloom-forming species (<3μm *Reticulofenestra* and *Gephyrocapsa* species) were common to abundant throughout, ranging from ~30-97%. The next most common species was medium-sized *Reticulofenestra* (3-5μm), which constituted ~2-47% of the
210 assemblage at Site U1463 and ~6-52% at Site U1464. *Sphenolithus* spp. reached up to ~20% at Site U1463 and ~23% at Site U1464, until it dramatically decreased at ~3.54 Ma, following the global pattern of extinction of the genus. Other commonly occurring species were *Calcidiscus* spp., that constituted up to ~7% at both sites, *Umbilicosphaera* spp., with relative abundances up to ~10% at Site U1463 and ~9% at Site U1464 and larger (>5μm) *Reticulofenestra* species, with percentages up to ~11% at Site U1463 and ~9% at Site U1464. Consistently present species, but with very low relative abundances, were

https://doi.org/10.5194/cp-2022-60
Preprint. Discussion started: 16 August 2022


Climate of the Past Discussions

Helicosphaera spp. and *Discoaster* spp. Total NAR ranged from ~2× 10^{10} to ~3× 10^{11} N/cm^2 kyr at Site U1463 and ~2× 10^{10} to ~2× 10^{11} N/cm^2 kyr at Site U1464.

Two time intervals can be identified that represent distinct changes in nannofossil assemblage composition and NAR of the most common species (Figures A1, A2). The first one occurred from 5.4–5.2 Ma and was characterized by a ~10% increase in relative abundance (and NAR) of bloom-forming species and a synchronous ~10% decrease in relative abundance (and NAR) of *Sphenolithus* spp. at both sites. The fact that the burial fluxes (NAR) changed in opposite direction supports the assumption that these taxonomic groups have distinct ecologies and were both affected simultaneously. At the same time, bulk sediment mass accumulation rates (MARs) do not demonstrate any notable, sustained change, indicating that the observed pattern in the assemblage composition was driven by changes in species' abundance (Figure A2). *Umbilicosphaera* spp. and large *Reticulofenestra* species had a distinctive low in relative abundances during this period, whereas *Calcidiscus* spp. was not significantly influenced.

The second interval occurred from 4.6–4.4 and represents a rapid decrease in total NAR, mainly driven by the decrease in abundance of small *Reticulofenestra* species (Karatsolis et al., 2020), as well as a basin-wide decrease in low-latitude paleoproductivity (Karatsolis et al., 2022). During this interval, other common species such as *Calcidiscus* spp. and *Umbilicosphaera* spp. demonstrated increased NAR and a stepwise increase in relative abundance (Figures A1 and A2). Large *Reticulofenestra* species virtually disappeared during this interval, following the rapid decrease in NAR of the smaller species of their genus (Figure A2). As NARs of small *Reticulofenestra* spp. decreased, the small *Gephyrocapsa* spp. species started to increase (~4.45–4.42 Ma) in percentage and became dominant from ~4.2 Ma until the end of the studied interval, with maximum NAR values of ~1 × 10^{11} N/cm^2 kyr at IODP Site U1463 and ~5 × 10^{10} N/ cm^2 kyr at IODP Site U1464, which corresponds to ~70% and ~60% of the total assemblage respectively. After ~4.4 Ma, NAR of *Sphenolithus* spp. bounced back to higher values, especially at IODP Site U1463, presenting distinct peaks that are centred at ~4.1 Ma and 3.7 Ma. This species' relative abundance increased too, reaching in cases values of >10%, although it never reached its latest Miocene maxima (Figure A1).

https://doi.org/10.5194/cp-2022-60
Preprint. Discussion started: 16 August 2022

Climate of the Past Discussions
Open Access
EGU

240 **3.2 Nannofossil stratification index (NSI)**

As is the case for the nannofossil assemblage compositions, changes in NSI correlate well between the two sites and covary throughout the studied interval (Figure 4). A stepwise decrease is observed from 5.4–5.2 Ma, which mirrors the overall decrease in relative abundance and NAR of *Sphenolithus* spp. and the synchronous increase in small *Reticulofenestra* species. After ~4.2 Ma, this surface water stratification proxy shows higher variation with small intervals of higher values (4.2-4 Ma
245 and 3.8-3.54 Ma), that correspond to peaks in relative abundance of *Sphenolithus* spp. Between 4 and 3.8 Ma, NSI demonstrates low values, whereas after 3.54 Ma, the last occurrence (LO) of *Sphenolithus* spp. makes the index non-applicable.

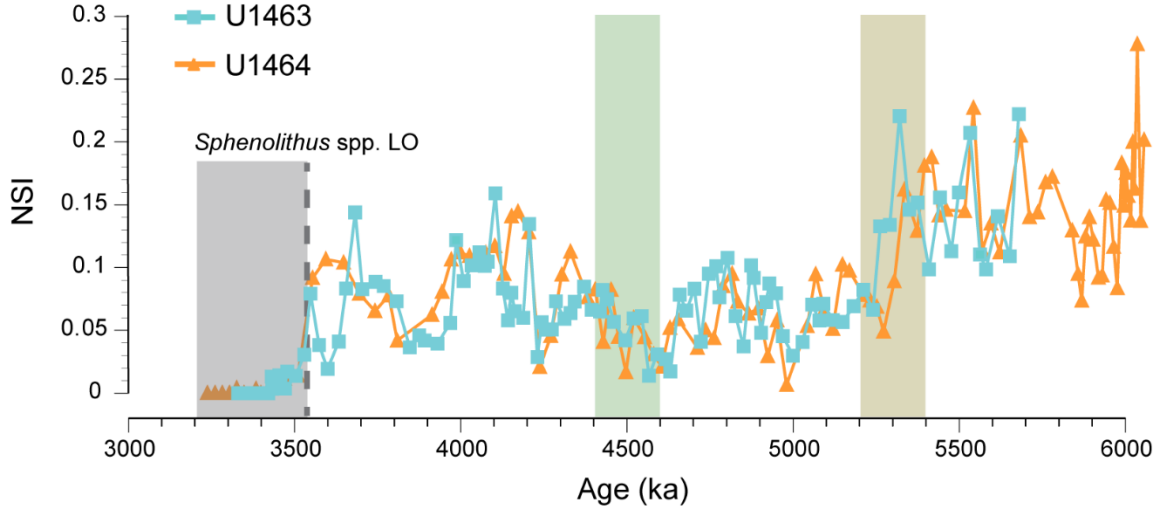

250 **Figure 4: Latest Miocene to early Pliocene nannofossil stratification index (NSI) at IODP Sites U1463 (light blue) and U1464 (orange). Brown shaded area represents the stepwise decrease in NSI and increase in NAR of bloom-forming species. Green shaded area represents the interval of significant decrease in PP and NAR of bloom-forming species. Dashed grey line indicates the Last Occurrence (LO) of *Sphenolithus* spp. during the early Pliocene (~3.54 Ma). Therefore, this NSI cannot be used for younger samples (grey shading).**

3.3 Correspondence Analysis (CA) and Shannon Diversity Index (H)

255 By color-coding the samples based on their age and major changes in the assemblage, namely distinct time intervals identified before 5.4-5.2 Ma and after 4.6–4.4 Ma (Figure 5), we test if any of the changes led to shifts in the relationship between relative abundances of species in multivariate space and therefore to significant restructuring of species compositions. Correspondence analysis at both sites mainly highlights the changes that occurred during 4.6–4.4 Ma, almost splitting the samples that belong to the period before the rapid decrease in NAR from those after that across the primary CA axis (Figure 5a, b). It also separates
260 and links the species that were more dominant before and after ~4.4 Ma with the respective interval of dominance (low angle from the (0,0) source between species and sample age). The separation occurs between species such as small *Reticulofenestra* and *Sphenolithus* spp. from small *Gephyrocapsa*, *Calcidiscus* spp. and *Umbilicosphaera* spp. (Figure 5). Medium *Reticulofenestra* appears to have a less clear affinity, being close to the primary axis and on opposite sides of it at IODP Site

https://doi.org/10.5194/cp-2022-60
Preprint. Discussion started: 16 August 2022

U1463 and U1464. This can probably be attributed to the fact that this species showed relatively stable relative abundances and two distinct peaks before and after the 4.6–4.4 Ma event (Figure B1), which could also explain the few before/after 4.4 Ma samples that fall on the same side of the axis (Figure 5a, b). Interestingly, species loadings and <4.4 Ma sample scores correlate well, and both appear to be situated further from the (0,0) source, demonstrating that the association of common species with the younger part of the record is stronger. Finally, the H index also demonstrates that the most distinct change, which collectively influenced the nannofossil species distribution, occurred from 4.6–4.4 Ma and was marked by a stepwise increase in diversity (Figure 6). Notably, no sustained change in diversity is observed during the interval of stepwise decrease in NSI (5.4–5.2 Ma; Figure 4).

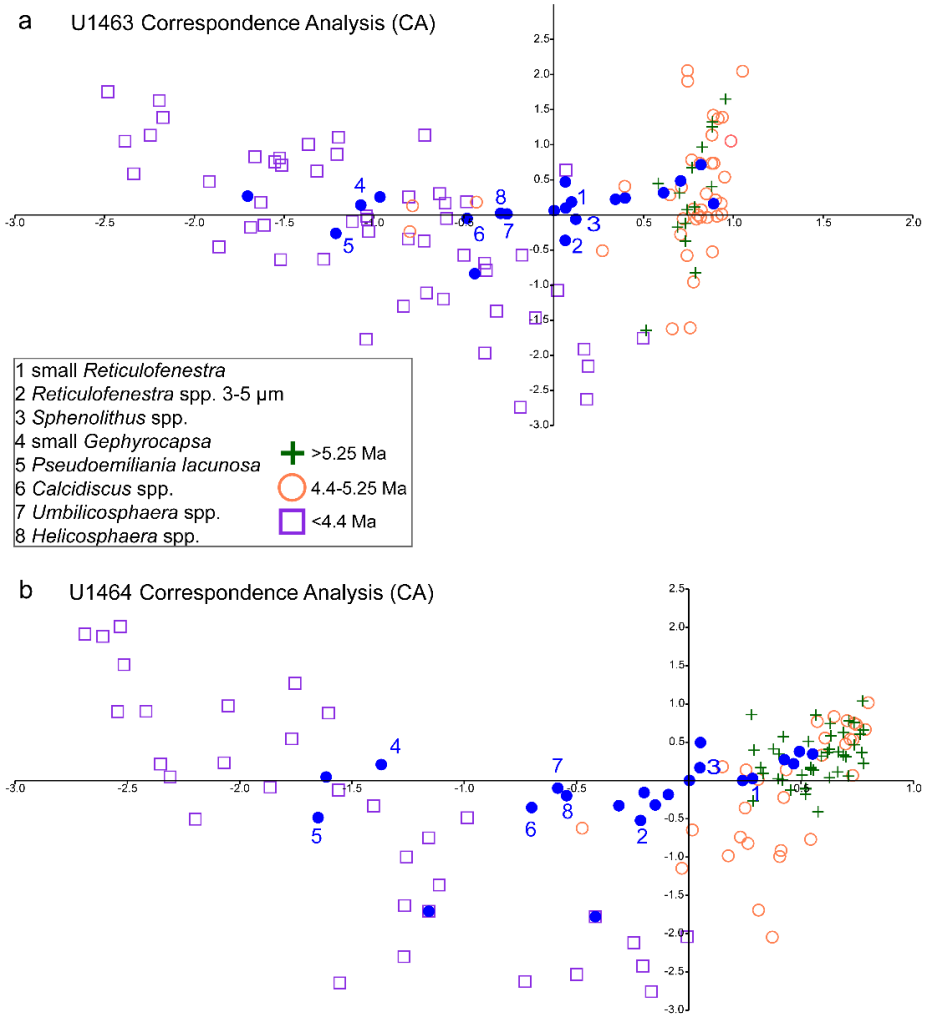

Figure 5: Correspondence Analysis (CA) for IODP Sites U1463 (a) and U1464 (b). Orange circles represent samples prior to 5.25 Ma and together with the green crosses constitute the records prior to the significant decrease in NAR that occurred at 4.6–4.4 Ma. Boxes in purple represent samples <4.4 Ma. Numbered blue points represent the most common nannofossil species.

https://doi.org/10.5194/cp-2022-60
Preprint. Discussion started: 16 August 2022

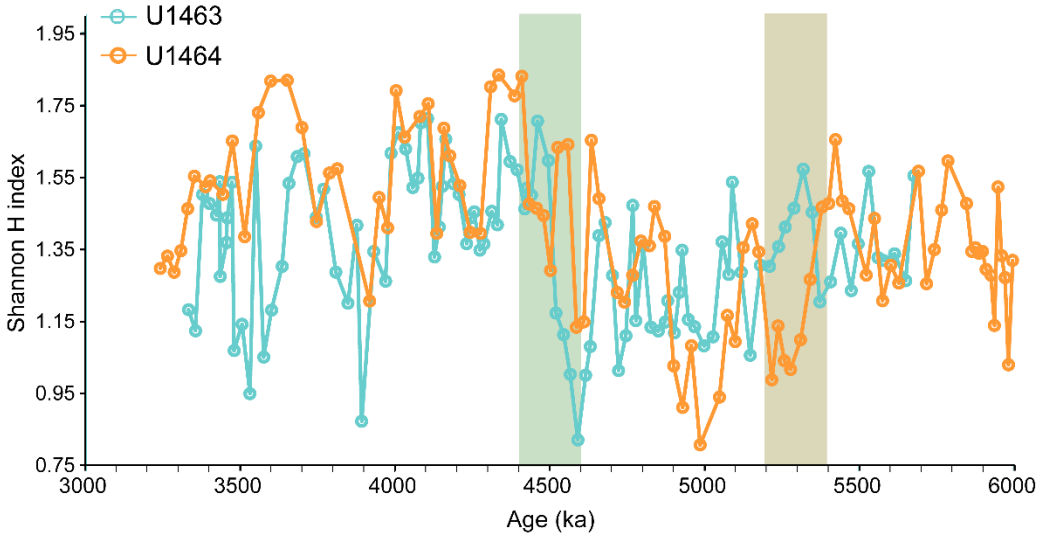

Figure 6: Shannon Diversity Index (H) calculated using PAST 4 software and plotted against sample age (ka) at IODP Sites U1463 (blue) and U1464 (orange). Brown shaded area represents the stepwise decrease in NSI and increase in NAR of bloom-forming species. Green shaded area represents the interval of significant decrease in PP and NAR of bloom-forming species.

3.4 Paleotemperature gradients

In general, the TEX_{86} record from IODP Site U1461 has been previously used as an indicator of temperature for the whole water column (0-200 m; He et al., 2021; Smith et al., 2013), whereas $U^{k'}_{37}$ and Mg/Ca have been used as indicators of SST for the eastern Indian Ocean (e.g., He et al., 2021; Karas et al., 2011); upper ~50 m of the water column). According to these previous interpretations, we label the gradients between $U^{k'}_{37}$ and Mg/Ca as ΔSST and the ones between TEX_{86} and Mg/Ca as ΔT. Four pairs of gradients were calculated, two between $U^{k'}_{37}$ SST at Site U1461 and Mg/Ca SSTs at ODP Site 763 and DSDP Site 214 ($\Delta SST_{U1461\text{-}763}$, $\Delta SST_{U1461\text{-}214}$), as well as two between TEX_{86} temperatures at Site U1461 and the same SSTs for the eastern Indian Ocean sites ($\Delta T_{U1461\text{-}763}$, $\Delta T_{U1461\text{-}214}$). All records demonstrate similar patterns and co-vary throughout the Pliocene and can be separated in three distinct intervals. The first one occurs before ~5.2 Ma, when all gradients have positive values, demonstrating that temperatures at Site U1461 were consistently higher at this time than those in the eastern Indian Ocean. Being the only one with more than 3 samples, $\Delta T_{U1461\text{-}763}$ is the most informative gradient for the interval >5.2 Ma and therefore for the latest Miocene. Between 6-5.2 Ma, this gradient has a median value of ~2 °C, which then becomes -0.6 °C for the interval between 5.2-2.5 Ma, driven by a cooling at Site U1461 and a warming at Site 763A (Figure 7). This indicates that TEX_{86} temperatures at Site U1461 transitioned from a phase of steadily warmer conditions to slightly cooler values compared to Site 763A. In general, ΔSST gradients are lower than ΔT, with median values of -0.2 and -0.5 °C for $\Delta SST_{U1461\text{-}763}$, $\Delta SST_{U1461\text{-}214}$ and -0.63 and -1.14 °C for $\Delta T_{U1461\text{-}763}$, $\Delta T_{U1461\text{-}214}$ respectively for the interval from 5.2-3.5 Ma (see Table D1). Median values also reveal that, both for the ΔSST and the ΔT records, gradients are generally higher between Site U1461 and DSDP Site 214 than those between U1461 and 763A. After 5.2 Ma and until ~4.3 Ma, gradients have negative values

https://doi.org/10.5194/cp-2022-60
Preprint. Discussion started: 16 August 2022

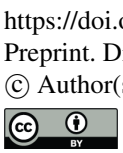

Climate of the Past Discussions

(reflecting lower temperatures over the shelf) and show small fluctuations between 0 and -2 °C, whereas after ~4.3 Ma fluctuations become more intense and vary significantly from ~ -3.5 to 2 °C. Despite this strong variation, positive gradient values never exceed the ones observed before 5.2 Ma and mostly remain negative, indicating that warmer conditions were prevailing in the eastern Indian Ocean, whereas waters over the shelf were generally cooler.

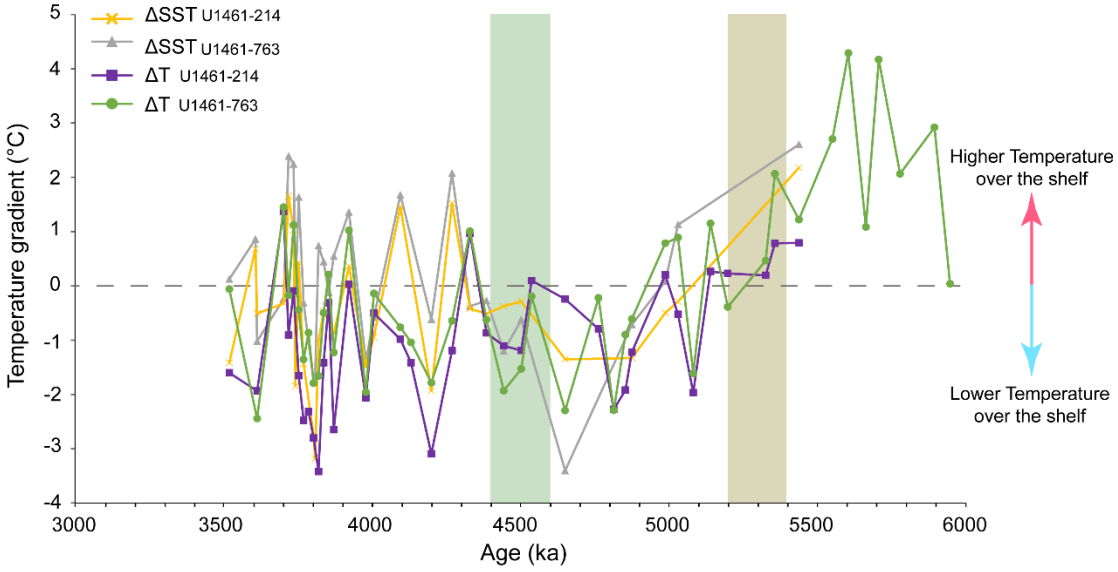

Figure 7: Temperature gradients (ΔT and ΔSST) between IODP Site U1461 (NW Australian shelf), ODP Site 763A (Exmouth Plateau) and DSDP Site 214 (eastern Indian Ocean). Gradients are calculated between the TEX_{86} and Mg/Ca records (ΔT) and between $U^{k'}_{37}$ and Mg/Ca records (ΔSST) for the interval 6-3.5 Ma. Horizontal grey dashed line indicates no difference in temperature (ΔT, ΔSST = 0°C). Brown shaded area represents the stepwise decrease in NSI and increase in NAR of bloom-forming species. Green shaded area represents the interval of significant decrease in PP and NAR of bloom-forming species.

4 Discussion

4.1 Water column mixing and nutrient availability on the NW Australian shelf

The common species comprising the NSI, namely small bloom-forming species and *Sphenolithus* spp., provided the bulk of the nannoplankton biomass and productivity and can therefore be expected to represent species that had broad ecological tolerances and the potential to record climate-biota interactions and feedbacks over long time intervals (e.g., Hannisdal et al., 2012; Henderiks et al., 2020). Additionally, since the nannofossil abundance in each sample represents an average, smoothed record over thousands of years, it would be impossible to directly infer changes in seasonal and interannual variation of the ITF and LC in a similar way that modern plankton observations and climate models do. Despite that, it can be expected that changes in ocean circulation or seasonality that significantly influenced the flow path of major boundary currents over the course of thousands of years, would be mirrored in the mean nannofossil assemblage, favouring taxa that benefited seasonally or interannually by the prevailing conditions. Therefore, the NSI can give us an indication of persistent overall changes in

https://doi.org/10.5194/cp-2022-60
Preprint. Discussion started: 16 August 2022


Climate of the Past Discussions

water column stratification and mixing, that could be driven by a long-term switch in seasonal dynamics, ITF flow or LC intensity during the latest Miocene to Pliocene.

On this basis, the NSI reveals a stepwise phase of reduction in stratification and intensified nutrient replenishment in the upper water column, that took place around the Miocene-Pliocene boundary (5.4-5.2 Ma; Figure 4). This suggests significant environmental changes during that time and a transition from a more tropical stratified environment to a modern-like dynamic shelfal area, favouring bloom-forming species over *Sphenolithus* spp. After its reduction, NSI never returned to its late Miocene levels, demonstrating that increased water column mixing was a prevailing regime in the area from 5.2-3.54 Ma, although an interval of overall higher NSI, with some variation and interchanging higher and lower phases can be observed from ~4.2 to 3.54 Ma (Figure 4).

Three possible mechanisms related to regional paleoclimate and the LC dynamics in the area could explain the observed pattern. The first one would suggest a strong effect of changes in upper water column stratification on primary productivity due to a LC acceleration, as it has been previously documented in a series of modern observational data and Pleistocene paleoclimatic records. Specifically, intensified LC activity has been linked to increased eddy formation that promotes enhanced productivity across the western Australian continental shelf (Auer et al., 2021; Feng et al., 2009; Furnas, 2007; Koslow et al., 2008; Thompson et al., 2011). This mechanism has also been proposed for other coastal areas influenced by boundary currents such as the southwestern Australian shelf (Harris et al., 1987; Koslow et al., 2008) and the Japanese coast (Kimura et al., 2000). Additionally, the modern observational and simulated data also show that the NW Australian shelf demonstrates increased water column mixing and phytoplankton productivity close to the shelf during austral winter when LC is stronger (Figures 2 and 3). Since the presence of the LC depends on steeper steric height gradients between the source areas and the southern latitudes, we hypothesize that such steepening intensified during the early Pliocene, triggering enhanced seasonal flow of this major boundary current. In turn, intensified eddy activity and vertical mixing during the winter season and a subsequent "pumping" of nutrients from the continental slope onto the outer continental shelf, generated the observed long-term patterns in NSI, as well as the increase in NAR of bloom-forming species (Figure A2).

A second mechanism that could explain the NSI decrease, is the overall increase in convective mixing across the continental shelf area. This could be the effect of intensified cooling in the upper water column, as well as intensified storm activity during the winter period, which are known to have the potential for generating blooms by mixing the water column and bringing nutrients to the euphotic zone (e.g Chen et al., 2020; Longhurst, 2001). This mechanism was proposed for modern winter blooms along the west coast of Australia, which have been attributed to mixing of the upper water column and a shoaling of the nutricline and chlorophyll maximum layer (Koslow et al., 2008).

The third mechanism comes in contrast to the first one and is based merely on the physical properties of the LC. According to that scenario, the warm SSTs and nutrient deficient waters that characterize the LC (Godfrey et al., 1986; Ridgway and Condie, 2004) should inhibit upwelling activity and stratify the water column, and therefore lead to overall decreased primary productivity, even across the continental shelf. Specifically, this relationship has been used to support the plausible LC activity in the NW Australian shelf from 6-4 Ma, based on the low concentrations in the sediment of isoGDGTs and C28–C30 sterols

https://doi.org/10.5194/cp-2022-60
Preprint. Discussion started: 16 August 2022


Climate of the Past Discussions

(He et al., 2021). Similarly, a cooling during the Pleistocene along the NW Australian shelf has been previously attributed to a slowing down of the LC that would have allowed for intensified regional upwelling (Smith et al., 2020). Following the latter scenario, the reduction in NSI that we observe would be the result of a LC weakening, that allowed for seasonal upwelling and nutrient enrichment in the upper water column. However, it is worth noting that a similar cooling and intensification of upwelling could be achieved by a long-term strengthening of the summer north-westerly winds that overcome the south-easterly trade winds and have the potential to generate seasonal upwelling.

4.2 Paleotemperature and inferred ocean circulation patterns

Temperature gradients between the eastern Indian Ocean and the NW Australian shelf sites further support significant changes in ocean circulation during the late Miocene to Pliocene and compliment the observed changes in the nannofossil assemblage. In general, the higher ΔT gradient (in absolute values) after 5.2 Ma compared to the ΔSST, support the hypothesis that TEX_{86} temperatures are influenced by a slightly deeper and cooler signal of the integrated upper 200m of the water column (He et al., 2021; Smith et al., 2013). Although these differences are consistent throughout the record, they are generally small and therefore in good accordance with the low gradient between the integrated water column temperature and the SST ($\Delta T_{TEX86-U^{k'}_{37}}$) for the interval between 6-3 Ma at IODP Site U1461 (median value of ~1.1°C; He et al., 2021). More importantly, the temperature differences derived from all proxies between the NW Australian shelf and the eastern Indian Ocean sites show similar variation and record a stepwise decrease of the temperature gradient between the two areas, driven by a cooling in the former area and a warming in the latter (Figure 8 a, b). The overall shift can be tracked by the median values of $\Delta T_{U1461-763}$ before and after 5.2 Ma, which suggest a shift of ~2.5°C that closes the temperature gap between the shelf and the eastern Indian Ocean, while flipping the temperature relationship between the two regions by making the latter one warmer. Similar temperatures across the NW Australian shelf and the eastern Indian Ocean indicate well-established ITF connectivity, in good agreement with the suggested warm and humid conditions that were prevailing in the area since the late Miocene (Christensen et al., 2017; Karatsolis et al., 2020). Interestingly, this change also coincides with the decrease in NSI from 5.4–5.2 Ma, suggesting a possible link between the changes in temperature and the stratification index (Figure 8 a, b), either by decreased tolerance of *Sphenolithus* spp. to relatively cooler temperatures, or through changes in nutrient availability due to intensified seasonal mixing and/or upwelling that favoured opportunistic species.

In principle, a cooling at Site U1461 could be explained either by cooler surface water that began to influence the area and decreased the average temperature, or by the weakening of the ITF and LC which would have allowed for seasonal upwelling of deeper, colder water to occur, or by a sustained increase in vertical mixing, that led to an overall decrease in temperature in the integrated upper water column. However, since evidence for significant restriction of the ITF or a switch of LC source are suggested to occur much later, towards the late Pliocene (e.g. Christensen et al., 2017; Karas et al., 2011; De Vleeschouwer et al., 2019), less stratification induced by intensified seasonality is the most probable scenario to have generated the observed changes in the average temperature signal. This would have resulted in a deeper mixed layer and increased eddy formation along the Australian shelf due to increased storm track activity during the winter season. Further evidence for the increased

https://doi.org/10.5194/cp-2022-60
Preprint. Discussion started: 16 August 2022

presence of the LC in the area comes from ODP Site 763A. Records from this site have been previously used to infer the presence of this boundary current in the geological past (e.g., Auer et al., 2019; Karas et al., 2011) and it is located in an area that has been commonly used to test LC activity through Ocean General Circulation models (Godfrey, 1996; Hirst and Godfrey, 1993). At ODP Site 763A, we observe a distinct increase in SST of ~2°C, a shift that would not be possible if the source of the LC had become cooler, or if the LC was weakened in order to accommodate the hypothesis of cooling in the shelfal area. At the same time, no warming is observed further offshore at DSDP Site 214, strengthening the hypothesis that ODP Site 763A tracks the more regional effect of the LC.

Combined, the changes in NSI and paleotemperatures could be explained by an overall intensification of seasonality and the related pressure gradients over NW Australia. Such intensification would translate in stronger trade winds during the winter and LC intensification and warming at ODP Site 763A. Meanwhile, the decrease in NSI could be generated either by a sustained increase in vertical mixing and eddy formation over the shelf during the winter season, or by the stronger reversal of the trade winds and monsoonal north-westerlies during the summer, which can promote regional upwelling. Both scenarios could be the result of an invigoration in seasonal extremes, marking the transition to a less tropical, less stratified environment and a significant shift in the paleoecological and paleoceanographic regime in the area (Regime 1 to Regime 2; Figure 8). The reverse scenario would apply for the periods before 5.4 Ma and (less intensely) after ~4.2 Ma, when higher NSI and the dominance of *Gephyrocapsa* spp., a bloom-forming group of species with increased tolerance to warmer and more stratified conditions, is observed. Further offshore, at ODP Site 763A, where the effect of continental shelf eddy formation and seasonal upwelling is weaker, the invigorated seasonal presence of the LC after ~5.4–5.2 Ma, is solely translated by an overall increase in SSTs.

Although the records investigated in this study do not allow for an extended evaluation of the driving mechanisms behind this regime shift, the globally elevated temperatures that marked the beginning of the Pliocene (~5.3 Ma; Fedorov et al., 2006) could have played a role in increasing monsoonal precipitation and tropical cyclones (Fedorov et al., 2010), therefore invigorating water column mixing in low latitudes. However, this warming was suggested to be an expression of a permanent El Niño state (Fedorov et al., 2006; Wara et al., 2005), which would contradict our argument of an intensified seasonal presence of the LC, since this current is expected to be significantly weaker under such conditions (e.g., Feng et al., 2003, 2009). When compared to other studies, our interpretation falls close to the hypothesis by He and others (2021), namely that the LC was active during the early Pliocene and from 6-4 Ma, before it weakened after ~4 Ma. On the other hand, De Vleeschouwer and others (2022) argued for a strong LC from ~4-3.7 Ma and a weaker phase from ~3.7-3.1 Ma, a reconstruction we cannot evaluate using the NSI because this index cannot be applied after 3.54 Ma (see Figure 3). More importantly, our study indicates the complex, differential effects that an intensification in seasonality and the LC would have had on the shelf and further offshore.

https://doi.org/10.5194/cp-2022-60
Preprint. Discussion started: 16 August 2022


Climate of the Past Discussions

4.3 Broader-scale changes in paleoproductivity and paleoecology

The studied time interval falls within a period of elevated biogenic sedimentation called the late Miocene to early Pliocene biogenic bloom (e.g., Dickens and Owen, 1999; Diester-Haass et al., 2005; Farrell et al., 1995; Hermoyian and Owen, 2001), which has been observed in numerous locations in all major oceans and potentially came to an end, at least in low latitudes, with a sharp decrease in PP that occurred between 4.6–4.4 Ma (Karatsolis et al., 2022). This global event was also expressed at Sites U1463 and U1464 by an abrupt decrease in nannofossil fluxes, as well as a significant restructuring of the nannofossil assemblage, as indicated by the CA (Figure 5) and the increase in H-index (Figure 6). Despite the relative abundance changes, small and medium-sized, bloom-forming coccolithophores dominated the assemblage throughout the studied interval. This could partially be explained by the constant supply of nutrients because of a steady terrigenous runoff (Karatsolis et al., 2020) onto the outer shelf/upper bathyal paleoenvironment, where the studied sites were situated during the "Humid Interval" (Christensen et al., 2017; Gallagher et al., 2017). However, it is also in good agreement with a basin-wide eutrophication event, that spanned from ~8.8 Ma (Imai et al., 2015) to ~3.5 Ma; during which *Reticulofenestra haqii* (medium sized) and *Reticulofenestra minuta* (small sized) assemblages dominated in the Indian Ocean (Young, 1990). Within the same period, a *Gephyrocapsa* dominance interval (acme) has been recorded from 4-3 Ma (Young, 1990), consistent with the observed progressive dominance of this species over the NW Australian that followed the termination of the biogenic bloom. However, we can now confirm that a complete dominance overturn was never achieved, as evident by the stepwise increase in diversity H-index at 4.6–4.4 Ma (Figure 6). This stepwise increase was partly supported by the increase in relative abundances of *Calcidiscus* spp. and *Umbilicosphaera* spp. (Figure A2), showing that these species were probably affected less by a basin-wide decrease in nutrient availability. At the same time, large *Reticulofenestra* species virtually disappeared, indicating an earlier shift towards the period of permanent dominance of smaller-sized placoliths, which has been proposed to have started at ~4–3.8 Ma, with evolutionary innovations such as the FO of *Pseudoemiliania* spp. (Figure C1) and LO of *Reticulofenestra pseudoumbilicus* (Aubry, 2007). Although significant assemblage changes occurred during the PP decrease, there was no major change in NSI (Figure 8). This supports the hypothesis that a broader change in nutrient availability occurred from 4.6–4.4 Ma, one that affected the abundance of dominant species as a whole and not the relative ecological success between common taxonomic groups (bloom-forming versus *Sphenolithus*). Additionally, the fact that the NSI remained unaltered underpins the potential of this index in decoupling long-term changes in relative dominance of species, controlled by regional ocean circulation patterns and seasonal water column mixing intensity, from large scale processes influencing PP through changes in the total ocean nutrient budget.

Further evidence for a decrease in fluxes or significant changes in the nannofossil assemblage, that would have marked the end of the biogenic bloom, are still limited for the rest of the Indian Ocean. Some observations of nannofossil export production from the open ocean ODP Site 757B (Figure 1) support a reduction in burial fluxes in good accordance with our results (Imai et al., 2020). Another study that investigated the nannofossil assemblage at ODP Site 762B (Figure 1), which is located closer to the shelf, recorded a significant decrease in nannofossil fluxes between ~4.2-3.9 Ma, with the nannofossil fluxes returning

https://doi.org/10.5194/cp-2022-60
Preprint. Discussion started: 16 August 2022

to higher values after that (Imai et al., 2015). However, it is important to note that the age models of these studies were based on few early Pliocene biostratigraphic tie-points, in contrast to the orbitally-tuned records presented herein. Therefore, the exact timing of events within <0.5 Ma precision should be considered with caution.

As far as it concerns the dominance of small *Gephyrocapsa*, several acme events of this species have been previously reported during the Pliocene and Pleistocene , but they seem to have been largely diachronous between ocean basins (Auer et al., 2019; Ballegeer et al., 2012; Gibbs et al., 2004; Marino and Flores, 2002). This supports the existence of several controlling mechanisms for the initiation of its dominance, age-model discrepancies, or a non-linear effect of a long-term ecological pressure across basins. Despite the diachronicity, it appears that small *Gephyrocapsa* had an opportunistic advantage in filling the available niches, and a paleoecological advantage to dominate the assemblage in several different paleoenvironments during the early Pliocene. Its increase in relative abundance can already be observed on the NW Australian shelf during, and directly after, the significant reduction in abundance of the opportunistic small *Reticulofenestra* species (4.6–4.4 Ma; Figure A2). However, small *Gephyrocapsa* clearly dominates after 4.2 Ma, and this could be related to our hypothesis of a relative increase in stratification and reduced seasonal mixing of the water column during that time. The subsequent widespread acme in the Indian Ocean (Young, 1990) could have been a result of overall, basin-wide warming and more stratified conditions, a hypothesis that is supported by the very high early Pliocene temperatures in both open ocean Indian Ocean sites (DSDP 214; ODP 763A; Karas et al., 2011) from ~4.3–3.5 Ma. Nevertheless, additional high-resolution nannofossil records are needed to confirm the diachronicity between small *Gephyrocapsa* acme events and the shifts in the nannofossil assemblages that marked the termination of the biogenic bloom.

https://doi.org/10.5194/cp-2022-60
Preprint. Discussion started: 16 August 2022

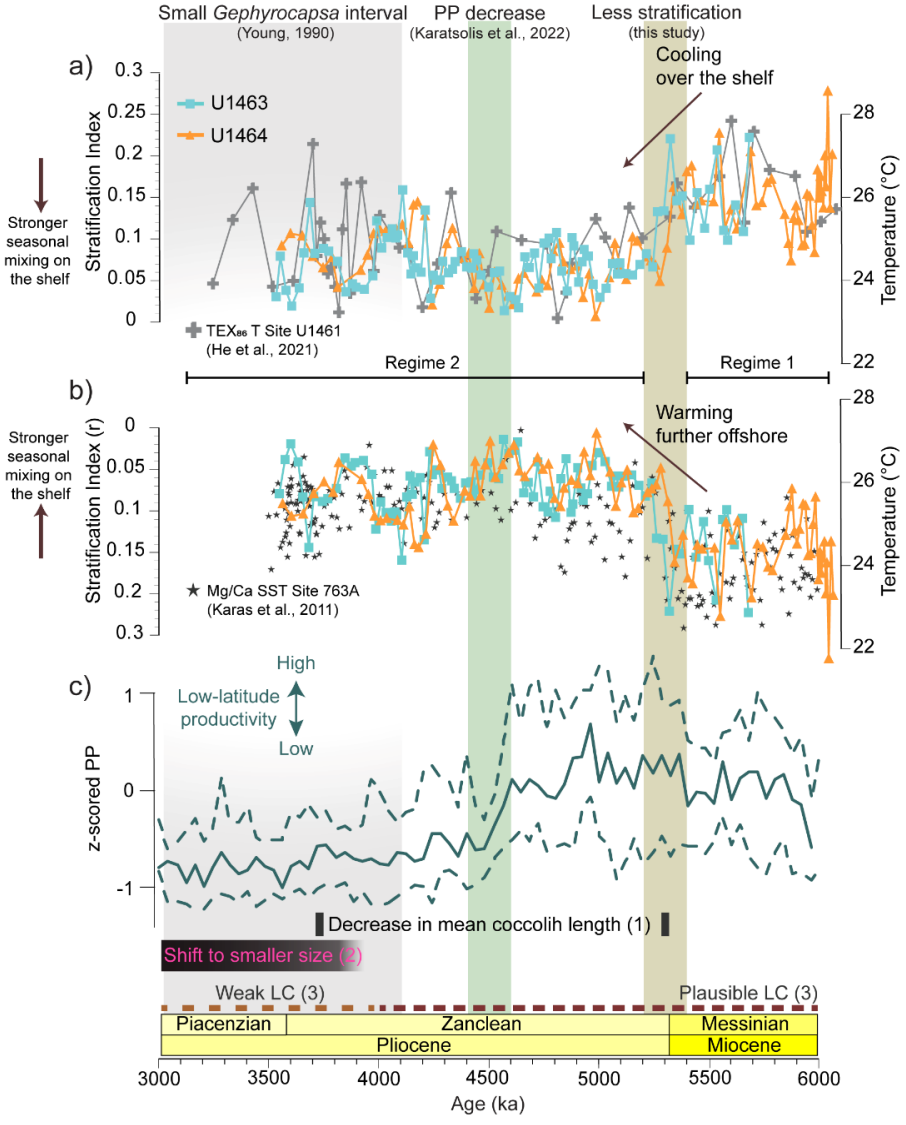

Figure 8. Correlation between paleotemperature proxies for the eastern Indian Ocean, water column stratification over the NW Australian shelf (NSI) and low-latitude paleoproductivity (PP). a) NSI (nannofossil stratification index; see methods) for IODP Sites U1463 (light blue) and U1464 (orange) and TEX_{86} derived temperature (°C) at IODP Site U1461 (He et al., 2021), located in the NW Australia shelf (grey line and crosses). NSI and *T. sacculifer* Mg/Ca derived SST (°C) at ODP Site 763A (Karas et al., 2011), located near the NW Australian shelf, but further offshore to the west in Exmouth Plateau (dark grey stars). Note reversed scale in y-axis of NSI c) Standardised median low latitude PP for all major ocean basins (Karatsolis et al., 2022). Dashed lines indicate the 15.9 and 84.1 percentiles (i.e. the central 68.2 percentiles) of the compiled data. Horizontal black bars indicate (1) distinct decrease in mean and maximum coccolith length, as recorded in the Indian Ocean (Young, 1990), (2) Period of permanent shift to smaller size coccoliths (Aubry 2007), (3) Suggested Leeuwin current (LC) intensity for the NW Australian shelf area (He et al., 2021). Horizontal black lines indicate the shift from Regime 1 to Regime 2. Vertical shaded areas indicate the stepwise decrease in NSI (brown), the decrease in low-latitude PP and nannofossil fluxes over the NW Australian shelf (green) and the small *Gephyrocapsa* dominance interval recorded in the Indian Ocean (gray; Young, 1990).

https://doi.org/10.5194/cp-2022-60
Preprint. Discussion started: 16 August 2022

5. Conclusion

The NW Australian shelf area during the late Miocene to Pliocene was influenced by an unrestricted Indonesian Throughflow and dominated by warm tropical waters under humid climatic conditions. Our investigations further constrained past regional ocean circulation and paleoproductivity between 6-3.5 Ma, using the nannofossil assemblage and the paleotemperature gradients between the shelfal area and the eastern Indian Ocean. The use of a nannofossil stratification index (NSI), which was based on the abundance of the most common calcareous nannofossil taxonomic groups, revealed a sustained shift in paleoclimatic and paleoceanographic regime between ~5.4-5.2 Ma. During that time, the water column over the NW Australian shelf transitioned from more stratified, tropical conditions to a dynamic shelfal environment with (seasonally) increased water column mixing and nutrient replenishment in the photic zone. This shift was possibly driven by more pronounced seasonal variations, expressed by intensified storm activity and eddy formation during the winter season and/or enhanced upwelling during the austral summer. The temperature gradients between the shelfal area and the pelagic domains of the Indian Ocean further strengthen this interpretation and suggest a more pronounced seasonal flow of the LC after ~5.2 Ma. In addition to regional ocean circulation, we explored the changes in the nannofossil assemblage that characterised the recently proposed termination of the late Miocene to early Pliocene biogenic bloom (4.6-4.4 Ma). Our data suggest that a restructuring of the nannofossil assemblage and an increase in diversity occurred during this interval, although the NSI was not significantly affected. The subsequent dominance of small *Gephyrocapsa* over the NW Australian shelf is interpreted as the expression of the broader dominance of this species in the Indian Ocean and its adaptation to the warm surface water conditions of the early Pliocene. This study highlights the differential response of the nannofossil assemblage to regional seasonal changes in the water column compared to broader-scale changes in paleoproductivity and the nutrient budget in the oceans. Questions remain on what mechanisms led to the proposed intensification in seasonality and the progressive dominance of small *Gephyrocapsa*, as well as what caused the changes in the nannofossil assemblage that marked the low-latitude decrease in PP in other ocean basins.

https://doi.org/10.5194/cp-2022-60
Preprint. Discussion started: 16 August 2022

Author contributions: B.T.K. conceived the study and performed the nannofossil counts and the data analysis, in close consultation with J.H. B.T.K. interpreted the results and wrote the first draft of this manuscript. J.H. contributed to a critical interpretation and discussion of the results and helped with the writing of the manuscript and the drafting of the figures.

Competing interests: The authors declare that they have no conflict of interest.

Acknowledgements
This research used samples and data provided by the International Ocean Discovery Program and is part of the first author's PhD studies, financially supported by the Swedish Research Council (Vetenskapsrådet; Project Grant VR 2016-04434 to J. H.). We are grateful to the co-chiefs, shipboard science party, and crew of the JOIDES Resolution for the successful operations during IODP Expedition 356.

Data availability
Additional data figures and tables that are part of this study can be found in the Appendix section. The raw data produced for this paper are publicly available at the Zenodo data repository (Karatsolis and Henderiks 2022, https://doi.org/10.5281/zenodo.6965870) and have also been submitted to PANGAEA, where they will become available upon publication.

https://doi.org/10.5194/cp-2022-60
Preprint. Discussion started: 16 August 2022

Climate of the Past Discussions
Open Access
EGU

Appendix A: Relative abundance and nannofossil accumulation rates of commonly occurring calcareous nannofossil species plotted against sample age.

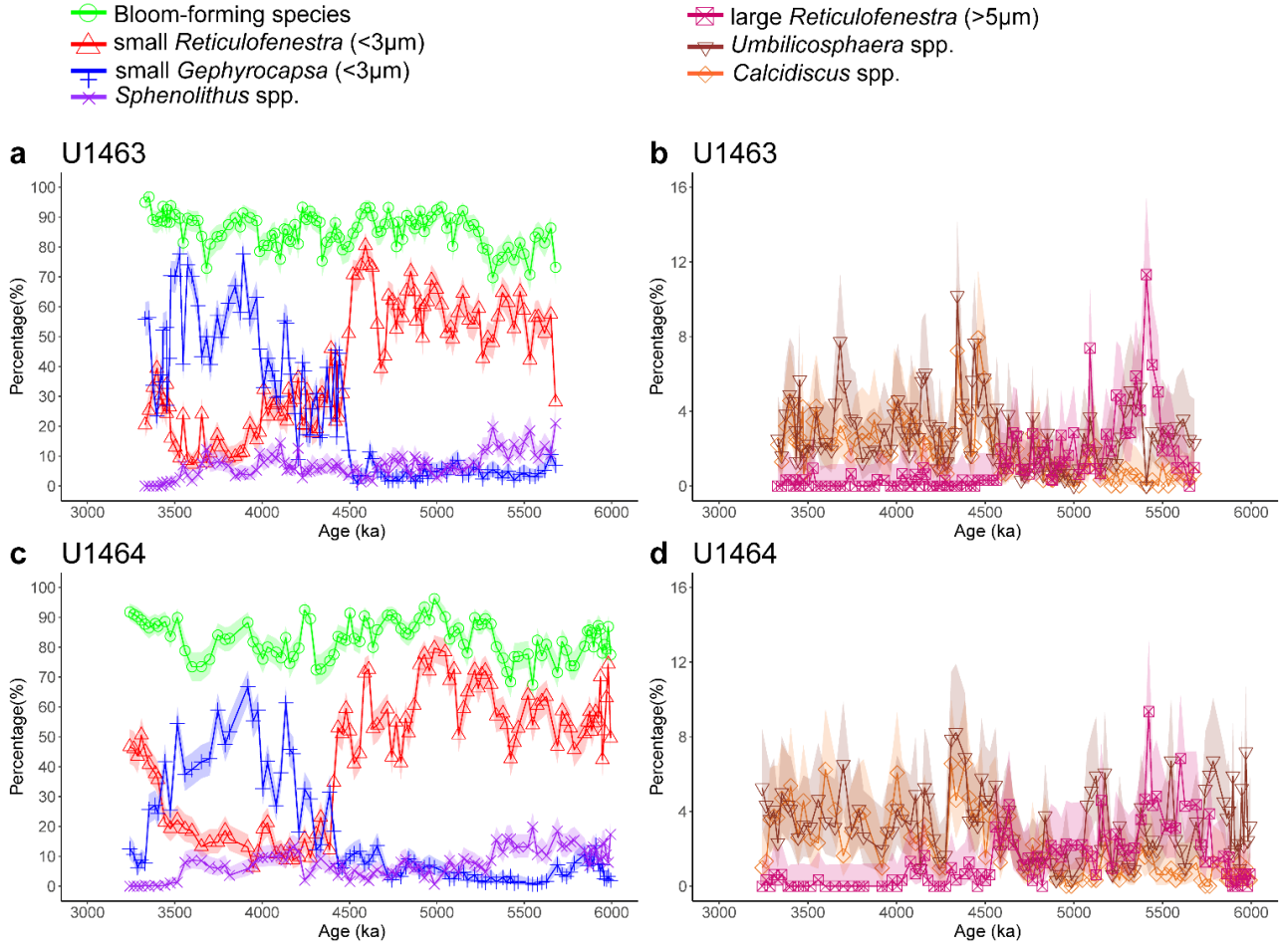

Figure A1: Latest Miocene to early Pliocene relative abundances (%) of commonly occurring calcareous nannofossil species from IODP Sites U1463 (a-b) and U1464 (c-d). Species are indicated in different colors. Bloom-forming species (<5μm *Reticulofenestra* and <3μm *Gephyrocapsa*; green), small (<3μm) *Reticulofenestra* (red), small (<3μm) *Gephyrocapsa* (blue), *Sphenolithus* spp. (purple), large (>5μm) *Reticulofenestra* (purple-pink), *Umbilicosphaera* spp. (brown) and *Calcidiscus* spp. (orange). Error bars represent 95% confidence intervals (see methods).

https://doi.org/10.5194/cp-2022-60
Preprint. Discussion started: 16 August 2022

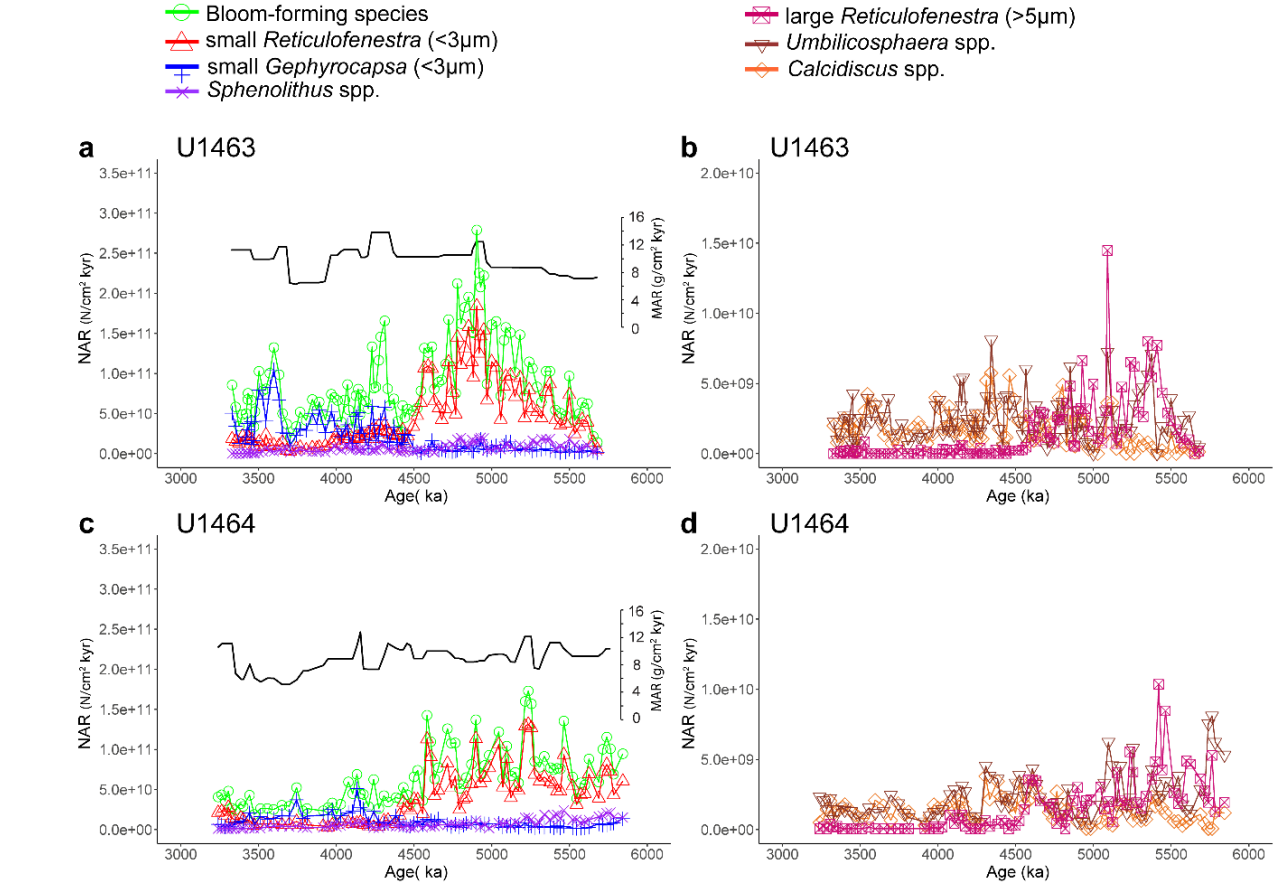

Figure A2: Latest Miocene to early Pliocene Nannofossil Accumulation Rates (NAR; N/cm^2 kyr) of commonly occurring calcareous nannofossil species from IODP Sites U1463 (a-b) and U1464 (c-d). Species are indicated in different colors. Bloom-forming species (<5µm *Reticulofenestra* and <3µm *Gephyrocapsa*; green), small (<3µm) *Reticulofenestra* (red), small (<3µm) *Gephyrocapsa* (blue), *Sphenolithus* spp. (purple), large (>5µm) *Reticulofenestra* (purple-pink), *Umbilicosphaera* spp. (brown) and *Calcidiscus* spp. (orange). Error bars of maximum replication error (15%; (Bordiga et al., 2015) were too small and therefore impaired the visual inspection of the figure. However, they are available as part of the source data of the paper. Superimposed on panel a) and b) is the bulk sediment MAR (g/cm^2 kyr) for IODP Sites U1463 and U1464 respectively.

https://doi.org/10.5194/cp-2022-60
Preprint. Discussion started: 16 August 2022

Climate of the Past Discussions
Open Access
EGU

Appendix B: Relative abundance of medium *Reticulofenestra* species plotted against age.

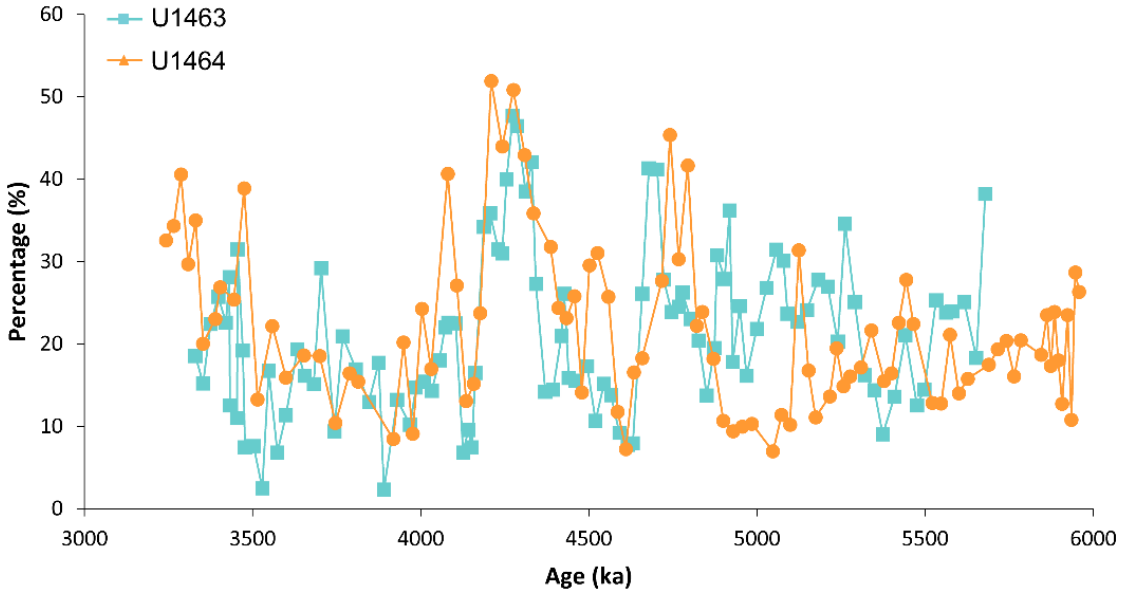

Figure B1: Relative abundances of medium (3-5µm) *Reticulofenestra* species plotted against sample age (ka) at IODP Sites U1463 (open circles; light blue line) and U1464 (closed circles; orange line). Distinct peaks (exceeding 40% of the assemblage) can be observed shortly before (~4.7 Ma) and after (~4.3 Ma) the 4.6–4.4 Ma decrease in PP.

https://doi.org/10.5194/cp-2022-60
Preprint. Discussion started: 16 August 2022

Climate of the Past Discussions

Appendix C: Absolute abundance of *Pseudoemiliania lacunosa* plotted against sample age.

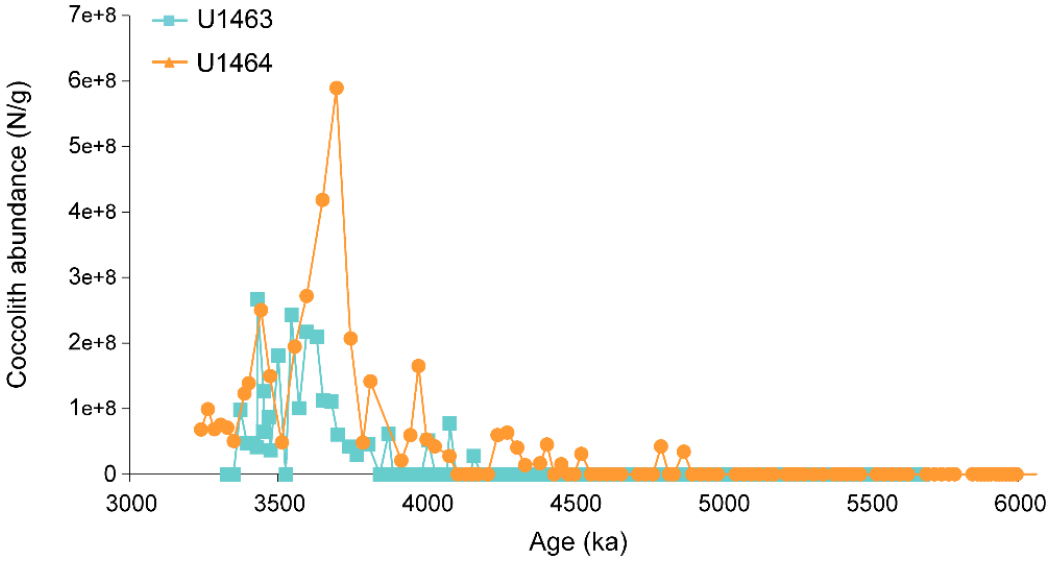

Figure C1: Absolute coccolith abundances (N/g × 10^8) of *Pseudoemiliania lacunosa* plotted against sample age (ka) at IODP Sites U1463 (squares; light blue line) and U1464 (circles; orange line).

https://doi.org/10.5194/cp-2022-60
Preprint. Discussion started: 16 August 2022

Climate of the Past Discussions

Appendix D: Summary of median age and temperature differences for the calculated paleotemperature gradients.

Table D1: Summary of median age and temperature differences for the calculated gradients between eastern Indian Ocean and NW Australian shelf sites. Initial records represent alkenone- ($U^{k'}_{37}$) and GDGT-based (TEX_{86}) temperature estimates from IODP Site U1461 (He et al., 2021) and planktonic foraminifera-based (Mg/Ca) for ODP Site 763A (Karas et al., 2011) and DSDP Site 214 (Karas et al., 2009).

Gradient (Sites)	Median Δage* (kyr) 6-3.5 Ma	Median ΔT (°C) 5.2-3.5 Ma	Median ΔT (°C) 6-5.2 Ma
U1461 ($U^{k'}_{37}$)-763	2.8	-0.2	
U1461 ($U^{k'}_{37}$)-214	9.6	-0.5	
U1461 (TEX_{86})-763	2.9	-0.6	2
U1461 (TEX_{86})-214	7.8	-1.15	

*Median Δage is calculated from the absolute difference between IODP U1461 sample ages and the closest available sample ages from ODP763/DSDP214

https://doi.org/10.5194/cp-2022-60
Preprint. Discussion started: 16 August 2022

References

Aubry, M.-P.: A major Pliocene coccolithophore turnover: Change in morphological strategy in the photic zone, Geol. Soc. Am., 424, 51, doi:https://doi.org/10.1130/SPE424, 2007.

Auer, G., De Vleeschouwer, D., Smith, R. A., Bogus, K., Groeneveld, J., Grunert, P., Castañeda, I. S., Petrick, B., Christensen, B., Fulthorpe, C., Gallagher, S. J. and Henderiks, J.: Timing and Pacing of Indonesian Throughflow Restriction and Its Connection to Late Pliocene Climate Shifts, Paleoceanogr. Paleoclimatology, 34(4), 635–657, doi:10.1029/2018PA003512, 2019.

Auer, G., Petrick, B., Yoshimura, T., Mamo, B. L., Reuning, L., Takayanagi, H., De Vleeschouwer, D. and Martinez-Garcia, A.: Intensified organic carbon burial on the Australian shelf after the Middle Pleistocene transition, Quat. Sci. Rev., 262, 106965, doi:10.1016/j.quascirev.2021.106965, 2021.

Ballegeer, A. M., Flores, J. A., Sierro, F. J. and Andersen, N.: Monitoring fluctuations of the Subtropical Front in the Tasman Sea between 3.45 and 2.45Ma (ODP site 1172), Palaeogeogr. Palaeoclimatol. Palaeoecol., 313–314, 215–224, doi:10.1016/j.palaeo.2011.11.001, 2012.

Beaufort, L., Lancelot, Y., Camberlin, P., Cayre, O., Vincent, E., Bassinot, F. and Labeyrie, L.: Insolation cycles as a major control of equatorial Indian Ocean primary production, Science (80-.)., 278(5342), 1451–1454, doi:10.1126/science.278.5342.1451, 1997.

Boeckel, B. and Baumann, K. H.: Vertical and lateral variations in coccolithophore community structure across the subtropical frontal zone in the South Atlantic Ocean, Mar. Micropaleontol., 67(3–4), 255–273, doi:10.1016/j.marmicro.2008.01.014, 2008.

Bolton, C. T., Hernández-Sánchez, M. T., Fuertes, M. Á., González-Lemos, S., Abrevaya, L., Mendez-Vicente, A., Flores, J. A., Probert, I., Giosan, L., Johnson, J. and Stoll, H. M.: Decrease in coccolithophore calcification and CO2 since the middle Miocene, Nat. Commun., 7, doi:10.1038/ncomms10284, 2016.

Bordiga, M., Bartol, M. and Henderiks, J.: Absolute nannofossil abundance estimates: Quantifying the pros and cons of different techniques, Rev. Micropaleontol., 58(3), 155–165, doi:10.1016/j.revmic.2015.05.002, 2015.

Bralower, T. J.: Evidence of surface water oligotrophy during the Paleocene-Eocene thermal maximum: Nannofossil assemblage data from Ocean Drilling Program Site 690, Maud Rise, Weddell Sea, Paleoceanography, 17(2), 583–592, doi:10.1029/2001pa000662, 2002.

Chen, M., Pattiaratchi, C. B., Ghadouani, A. and Hanson, C.: Influence of Storm Events on Chlorophyll Distribution Along the Oligotrophic Continental Shelf Off South-Western Australia, Front. Mar. Sci., 7(May), 1–19, doi:10.3389/fmars.2020.00287, 2020.

Christensen, B. A., Renema, W., Henderiks, J., De Vleeschouwer, D., Groeneveld, J., Castañeda, I. S., Reuning, L., Bogus, K., Auer, G., Ishiwa, T., McHugh, C. M., Gallagher, S. J., Fulthorpe, C. S., Mamo, B. L., Kominz, M. A., McGregor, H. V., Petrick, B. F., Takayanagi, H., Levin, E., Korpanty, C. A., Potts, D. C., Baranwal, S., Franco, D. R., Gurnis, M., Haller, C., He, Y., Himmler, T., Iwatani, H., Jatiningrum, R. S., Lee, E. Y., Rastigar, A. and Zhang, W.: Indonesian Throughflow drove Australian climate from humid Pliocene to arid Pleistocene, Geophys. Res. Lett., 44(13), 6914–6925, doi:10.1002/2017GL072977, 2017.

D'Adamo, N., Fandry, C., Buchan, S. and Domingues, C.: Northern sources of the Leeuwin Current and the "holloway Current" on the North West Shelf, J. R. Soc. West. Aust., 92(2), 53–66, 2009.

De Vleeschouwer, D., Petrick, B. F. and Martínez-García, A.: Stepwise Weakening of the Pliocene Leeuwin Current, Geophys. Res. Lett., 46(14), 8310–8319, doi:10.1029/2019GL083670, 2019.

De Vleeschouwer, D., Peral, M., Marchegiano, M., Füllberg, A., Meinicke, N., Pälike, H., Auer, G., Petrick, B., Snoeck, C., Goderis, S. and Claeys, P.: Plio-Pleistocene Perth Basin water temperatures and Leeuwin Current dynamics (Indian Ocean) derived from oxygen and clumped-isotope paleothermometry, Clim. Past, 18(5), 1231–1253, doi:10.5194/cp-18-1231-2022, 2022.

https://doi.org/10.5194/cp-2022-60
Preprint. Discussion started: 16 August 2022

Dickens, G. R. and Owen, R. M.: The Latest Miocene-Early Pliocene biogenic bloom: A revised Indian Ocean perspective, Mar. Geol., 161(1), 75–91, doi:10.1016/S0025-3227(99)00057-2, 1999.

Diester-Haass, L., Billups, K. and Emeis, K. C.: In search of the late Miocene-early Pliocene "biogenic bloom" in the Atlantic Ocean (Ocean Drilling Program Sites 982, 925, and 1088), Paleoceanography, 20(4), 1–13, doi:10.1029/2005PA001139, 2005.

Du, Y. and Qu, T.: Three inflow pathways of the Indonesian throughflow as seen from the simple ocean data assimilation, Dyn. Atmos. Ocean., 50(2), 233–256, doi:10.1016/j.dynatmoce.2010.04.001, 2010.

Farrell, J. W., Raffi, I., Janecek, T. C., Murray, D. W., Levitan, M., Dadey, K. A., Emeis, K.-C., Lyle, M., Flores, J.-A. and Hovan, S.: Late Neogene Sedimentation Patterns in the Eastern Equatorial Pacific, Proc. Ocean Drill. Program, 138 Sci. Results, (August), doi:10.2973/odp.proc.sr.138.143.1995, 1995.

Fedorov, A. V., Dekens, P. S., McCarthy, M., Ravelo, A. C., DeMenocal, P. B., Barreiro, M., Pacanowski, R. C. and Philander, S. G.: The pliocene paradox (mechanisms for a permanent El Niño), Science (80-.)., 312(5779), 1485–1489, doi:10.1126/science.1122666, 2006.

Fedorov, A. V., Brierley, C. M. and Emanuel, K.: Tropical cyclones and permanent El Niño in the early pliocene epoch, Nature, 463(7284), 1066–1070, doi:10.1038/nature08831, 2010.

Feng, M., Meyers, G., Pearce, A. and Wijffels, S.: Annual and interannual variations of the Leeuwin Current at 32°S, J. Geophys. Res. Ocean., 108(11), doi:10.1029/2002jc001763, 2003.

Feng, M., Waite, A. M. and Thompson, P. A.: Climate variability and ocean production in the Leeuwin Current system off the west coast of Western Australia, J. R. Soc. West. Aust., 92(2), 67–81, 2009.

Flores, J. A., Bárcena, M. A. and Sierro, F. J.: Ocean-surface and wind dynamics in the Atlantic Ocean off Northwest Africa during the last 140 000 years, Palaeogeogr. Palaeoclimatol. Palaeoecol., 161(3–4), 459–478, doi:10.1016/S0031-0182(00)00099-7, 2000.

Furnas, M.: Intra-seasonal and inter-annual variations in phytoplankton biomass, primary production and bacterial production at North West Cape, Western Australia: Links to the 1997-1998 El Niño event, Cont. Shelf Res., 27(7), 958–980, doi:10.1016/j.csr.2007.01.002, 2007.

Gallagher, S. J., Wallace, M. W., Li, C. L., Kinna, B., Bye, J. T., Akimoto, K. and Torii, M.: Neogene history of the West Pacific Warm Pool, Kuroshio and Leeuwin currents, Paleoceanography, 24(1), doi:10.1029/2008PA001660, 2009.

Gallagher, S. J., Fulthorpe, C. S., Bogus, K., Auer, G., Baranwal, S., Castañeda, I. S., Christensen, B. A., De Vleeschouwer, D., Franco, D. R., Groeneveld, J., Gurnis, M., Haller, C., He, Y., Henderiks, J., Himmler, T., Ishiwa, T., Iwatani, H., Jatiningrum, R. S., Kominz, M. A., Korpanty, C. A., Lee, E. Y., Levin, E., Mamo, B. L., McGregor, H. V., McHugh, C. M., Petrick, B. F., Potts, D. C., Rastegar Lari, A., Renema, W., Reuning, L., Takayanagi, H. and Zhang, W.: Expedition 356 summary, , 356(February), doi:10.14379/iodp.proc.356.101.2017, 2017.

Gibbs, S., Shackleton, N. and Young, J.: Orbitally forced climate signals in mid-Pliocene nannofossil assemblages, Mar. Micropaleontol., 51(1–2), 39–56, doi:10.1016/j.marmicro.2003.09.002, 2004.

Gibbs, S. J., Young, J. R., Bralower, T. J. and Shackleton, N. J.: Nannofossil evolutionary events in the mid-Pliocene: An assessment of the degree of synchrony in the extinctions of Reticulofenestra pseudoumbilicus and Sphenolithus abies, Palaeogeogr. Palaeoclimatol. Palaeoecol., 217(1–2), 155–172, doi:10.1016/j.palaeo.2004.11.005, 2005.

Gibbs, S. J., Stoll, H. M., Bown, P. R. and Bralower, T. J.: Ocean acidification and surface water carbonate production across the Paleocene-Eocene thermal maximum, Earth Planet. Sci. Lett., 295(3–4), 583–592, doi:10.1016/j.epsl.2010.04.044, 2010.

Godfrey, J. S.: The effect of the Indonesian throughflow on ocean circulation and heat exchange with the atmosphere: A review, J. Geophys. Res. Ocean., 101(C5), 12217–12237, doi:10.1029/95JC03860, 1996.

Godfrey, J. S. and Ridgway, K. R.: The Large-Scale Environment of the Poleward-Flowing Leeuwin Current, Western

https://doi.org/10.5194/cp-2022-60
Preprint. Discussion started: 16 August 2022

Australia: Longshore Steric Height Gradients, Wind Stresses and Geostrophic Flow, J. Phys. Oceanogr., 15(5), 481–495, 1985.

Godfrey, J. S., Vaudrey, D. J. and Hahn, S. D.: Observations of the Shelf-Edge Current South of Australia, Winter 1982, J. Phys. Oceanogr., 16(4), 668–679, 1986.

Gordon, A. L., Ma, S., Olson, D. B., Hacker, P., Ffield, A., Talley, L. D., Wilson, D. and Baringer, M.: Advection and diffusion of Indonesian throughflow water within the Indian Ocean South Equatorial Current, Geophys. Res. Lett., 24(21), 2573–2576, doi:10.1029/97GL01061, 1997.

Groeneveld, J., De Vleeschouwer, D., McCaffrey, J. C. and Gallagher, S. J.: Dating the Northwest Shelf of Australia since the Pliocene, Geochemistry, Geophys. Geosystems, 22(3), 1–20, doi:10.1029/2020GC009418, 2021.

Hammer, Ø., Harper, D. A. T. and Ryan, P. D.: Past: Paleontological Statistics Software Package for education and data analysis., , 4, 1–9, 2001.

Hannisdal, B., Henderiks, J. and Liow, L. H.: Long-term evolutionary and ecological responses of calcifying phytoplankton to changes in atmospheric CO 2, Glob. Chang. Biol., 18(12), 3504–3516, doi:10.1111/gcb.12007, 2012.

Haq, B. U.: Biogeographic history of Miocene calcareous nannoplankton and paleoceanography of the Atlantic Ocean., Micropaleontology, 26(4), 414–443, doi:10.2307/1485353, 1980.

Haq, B. U. and Lohmann, G. P.: Early Cenozoic calcareous nannoplankton biogeography of the Atlantic Ocean, Mar. Micropaleontol., 1, 119–194, 1976.

Harlay, J., Borges, A. V., Van Der Zee, C., Delille, B., Godoi, R. H. M., Schiettecatte, L. S., Roevros, N., Aerts, K., Lapernat, P. E., Rebreanu, L., Groom, S., Daro, M. H., Van Grieken, R. and Chou, L.: Biogeochemical study of a coccolithophore bloom in the northern Bay of Biscay (NE Atlantic Ocean) in June 2004, Prog. Oceanogr., 86(3–4), 317–336, doi:10.1016/j.pocean.2010.04.029, 2010.

Harris, G., Nilsson, C., Clementson, L. and Thomas, D.: The water masses of the east coast of Tasmania: Seasonal and interannual variability and the influence on phytoplankton biomass and productivity, Aust. J. Mar. Freshw. Res., 38(5), 569–590, 1987.

He, Y., Wang, H. and Liu, Z.: Development of the Leeuwin Current on the northwest shelf of Australia through the Pliocene-Pleistocene period, Earth Planet. Sci. Lett., 559, 116767, doi:10.1016/j.epsl.2021.116767, 2021.

Henderiks, J., Bartol, M., Pige, N., Karatsolis, B. T. and Lougheed, B. C.: Shifts in Phytoplankton Composition and Stepwise Climate Change During the Middle Miocene, Paleoceanogr. Paleoclimatology, 35(8), doi:10.1029/2020PA003915, 2020.

Hermoyian, C. S. and Owen, R. M.: Late Miocene-early Pliocene biogenic bloom: Evidence from low-productivity regions of the Indian and Atlantic oceans, Paleoceanography, 16(1), 95–100, doi:10.1029/2000PA000501, 2001.

Hirst, G. and Godfrey, J. S.: The Role of Indonesian Throughflow in a Global Ocean GCM, J. Phys. Oceanogr., 23(6), 1057–1086, 1993.

Holloway, P. E. and Nye, H. .: Leeuwin current and wind distributions on the southern part of the Australian North West Shelf between January 1982 and July 1983, Mar. Freshw. Res., 36, 123–137, 1985.

Imai, R., Farida, M., Sato, T. and Iryu, Y.: Evidence for eutrophication in the northwestern Pacific and eastern Indian oceans during the Miocene to Pleistocene based on the nannofossil accumulation rate, Discoaster abundance, and coccolith size distribution of Reticulofenestra, Mar. Micropaleontol., 116, 15–27, doi:10.1016/j.marmicro.2015.01.001, 2015.

Imai, R., Sato, T., Chiyonobu, S. and Iryu, Y.: Reconstruction of Miocene to Pleistocene sea-surface conditions in the eastern Indian Ocean on the basis of calcareous nannofossil assemblages from ODP Hole 757B, Isl. Arc, 29(1), doi:10.1111/iar.12373, 2020.

Karas, C., Nürnberg, D., Gupta, A. K., Tiedemann, R., Mohan, K. and Bickert, T.: Mid-Pliocene climate change amplified by a switch in Indonesian subsurface throughflow, Nat. Geosci., 2(6), 434–438, doi:10.1038/ngeo520, 2009.

https://doi.org/10.5194/cp-2022-60
Preprint. Discussion started: 16 August 2022

Karas, C., Nürnberg, D., Tiedemann, R. and Garbe-Schönberg, D.: Pliocene Indonesian Throughflow and Leeuwin Current dynamics: Implications for Indian Ocean polar heat flux, Paleoceanography, 26(2), 1–9, doi:10.1029/2010PA001949, 2011.

Karatsolis, B-Th. and Henderiks, J., (2022). Late Miocene to Pliocene calcareous nannofossil assemblage records and paleotemperature gradients from the NW Australian shelf (IODP Sites U1463, U1464) [Data set]. https://doi.org/10.5281/zenodo.6965870

Karatsolis, B. –. T., Lougheed, B. C., De Vleeschouwer, D. and Henderiks, J.: Abrupt conclusion of the late Miocene-early Pliocene biogenic bloom at 4.6-4.4 Ma, Nat. Commun., 13(1), 1–9, doi:10.1038/s41467-021-27784-6, 2022.

Karatsolis, B. T., De Vleeschouwer, D., Groeneveld, J., Christensen, B. and Henderiks, J.: The Late Miocene to Early Pliocene "Humid Interval" on the NW Australian Shelf: Disentangling climate forcing from regional basin evolution, Paleoceanogr. Paleoclimatology, 35(9), doi:10.1029/2019PA003780, 2020.

Kendrick, G. A., Goldberg, N. A., Harvey, E. S. and McDonald, J.: Historical and contemporary influence of the Leeuwin Current on the marine biota of the southwestern Australian continental shelf and the Recherche Archipelago, J. R. Soc. West. Aust., 92(2), 211–219, 2009.

Kimura, S., Nakata, H. and Okazaki, Y.: Biological production in meso-scale eddies caused by frontal disturbances of the Kuroshio Extension, ICES J. Mar. Sci., 57(1), 133–142, doi:10.1006/jmsc.1999.0564, 2000.

Koch, C. and Young, J. R.: A simple weighing and dilution technique for determining absolute abundances of coccoliths from sediment samples, J. Nannoplankt. Res., 29(1), 67–69, 2007.

Koslow, J. A., Pesant, S., Feng, M., Pearce, A., Fearns, P., Moore, T., Matear, R. and Waite, A.: The effect of the Leeuwin Current on phytoplankton biomass and production off Southwestern Australia, J. Geophys. Res. Ocean., 113(7), doi:10.1029/2007JC004102, 2008.

Longhurst, A.: A major seasonal phytoplankton bloom in the Madagascar Basin, Deep. Res. Part I Oceanogr. Res. Pap., 48(11), 2413–2422, doi:10.1016/S0967-0637(01)00024-3, 2001.

Marino, M. and Flores, J. A.: Miocene to Pliocene calcareous nannofossil biostratigraphy at ODP Leg 177 Sites 1088 and 1090, Mar. Micropaleontol., 45(3–4), 291–307, doi:10.1016/S0377-8398(02)00033-6, 2002.

O'Dea, S. A., Gibbs, S. J., Bown, P. R., Young, J. R., Poulton, A. J., Newsam, C. and Wilson, P. A.: Coccolithophore calcification response to past ocean acidification and climate change, Nat. Commun., 5, 1–7, doi:10.1038/ncomms6363, 2014.

Okada, H. and Wells, P.: Late quaternary nannofossil indicators of climate change in two deep-sea cores associated with the Leeuwin Current off Western Australia, Palaeogeogr. Palaeoclimatol. Palaeoecol., 131(3–4), 413–432, doi:10.1016/S0031-0182(97)00014-X, 1997.

Poulton, A. J., Stinchcombe, M. C., Achterberg, E. P., Bakker, D. C. E., Dumousseaud, C., Lawson, H. E., Lee, G. A., Richier, S., Suggett, D. J. and Young, J. R.: Coccolithophores on the north-west European shelf: Calcification rates and environmental controls, Biogeosciences, 11(14), 3919–3940, doi:10.5194/bg-11-3919-2014, 2014.

Ridgway, K. R. and Condie, S. A.: The 5500-km-long boundary flow off western and southern Australia, J. Geophys. Res. C Ocean., 109(4), 1–18, doi:10.1029/2003JC001921, 2004.

Ridgway, K. R. and Godfrey, J. S.: The source of the Leeuwin Current seasonality, J. Geophys. Res. Ocean., 120(10), 6843–6864, doi:10.1002/2015JC011049.Received, 2015.

Shannon, C. E.: A Mathematical Theory of Communication, Bell Syst. Tech. J., 27(3), 379–423, doi:10.1002/j.1538-7305.1948.tb01338.x, 1948.

Sharples, J., Moore, C. M., Hickman, A. E., Holligan, P. M., Tweddle, J. F., Palmer, M. R. and Simpson, J. H.: Internal tidal mixing as a control on continental margin ecosystems, Geophys. Res. Lett., 36(23), 1–5, doi:10.1029/2009GL040683, 2009.

Smith, M., De Deckker, P., Rogers, J., Brocks, J., Hope, J., Schmidt, S., Lopes dos Santos, R. and Schouten, S.: Comparison of U37K', TEX86H and LDI temperature proxies for reconstruction of south-east Australian ocean temperatures, Org.

https://doi.org/10.5194/cp-2022-60
Preprint. Discussion started: 16 August 2022

Geochem., 64, 94–104, doi:10.1016/j.orggeochem.2013.08.015, 2013.

Smith, R. A., Castañeda, I. S., Groeneveld, J., De Vleeschouwer, D., Henderiks, J., Christensen, B. A., Renema, W., Auer, G., Bogus, K., Gallagher, S. J. and Fulthorpe, C. S.: Plio-Pleistocene Indonesian Throughflow Variability Drove Eastern Indian Ocean Sea Surface Temperatures, Paleoceanogr. Paleoclimatology, 35(10), 1–20, doi:10.1029/2020PA003872, 2020.

Suchéras-Marx, B., Escarguel, G., Ferreira, J. and Hammer, Ø.: Statistical confidence intervals for relative abundances and abundance-based ratios: Simple practical solutions for an old overlooked question, Mar. Micropaleontol., 151, doi:10.1016/j.marmicro.2019.101751, 2019.

Takahashi, K. and Okada, H.: The paleoceanography for the last 30,000 years in the Southeastern Indian Ocean by means of calcareous nannofossils, Mar. Micropaleontol., 40(1–2), 83–103, doi:10.1016/S0377-8398(00)00033-5, 2000.

Thierstein, H. R. and Young, J. R.: Coccolithophores, Springer, Berlin, Heidelberg., 2004.

Thompson, P. A., Pesant, S. and Waite, A. M.: Contrasting the vertical differences in the phytoplankton biology of a dipole pair of eddies in the south-eastern Indian Ocean, Deep. Res. Part II Top. Stud. Oceanogr., 54(8–10), 1003–1028, doi:10.1016/j.dsr2.2006.12.009, 2007.

Thompson, P. A., Wild-Allen, K., Lourey, M., Rousseaux, C., Waite, A. M., Feng, M. and Beckley, L. E.: Nutrients in an oligotrophic boundary current: Evidence of a new role for the Leeuwin Current, Prog. Oceanogr., 91(4), 345–359, doi:10.1016/j.pocean.2011.02.011, 2011.

Van Oostende, N., Harlay, J., Vanelslander, B., Chou, L., Vyverman, W. and Sabbe, K.: Phytoplankton community dynamics during late spring coccolithophore blooms at the continental margin of the Celtic Sea (North East Atlantic, 2006–2008), Progress in Oceanography, Prog. Oceanogr., 104, 1–16, 2012.

Wade, B. S. and Bown, P. R.: Calcareous nannofossils in extreme environments: The Messinian Salinity Crisis, Polemi Basin, Cyprus, Palaeogeogr. Palaeoclimatol. Palaeoecol., 233(3–4), 271–286, doi:10.1016/j.palaeo.2005.10.007, 2006.

Wara, M. W., Ravelo, A. C. and Delaney, M. L.: Climate change: Permanent El Niño-like conditions during the Pliocene warm period, Science (80-.)., 309(5735), 758–761, doi:10.1126/science.1112596, 2005.

Young, J.: Size variation of Neogene Reticulofenestra coccoliths from Indian Ocean DSDP Cores, J. Micropalaeontology, 9(1), 71–85, doi:10.1144/jm.9.1.71, 1990.